# Which One Among Aspartyl Protease, Metallopeptidase, and Artificial Metallopeptidase is the Most Efficient Catalyst in Peptide Hydrolysis?

**Ram Prasad Bora, Arghya Barman, Xiaoxia Zhu, Mehmet Ozbil, and Rajeev Prabhakar***

*Department of Chemistry, University of Miami, 1301 Memorial Drive, Coral Gables, Florida 33146*

*Received: May 11, 2010; Revised Manuscript Received: June 30, 2010*

In this comparative DFT study, the hydrolysis of a peptide bond (Phe1-Phe2) by the following three types of catalysts has been studied: (1) $\beta$-secretase (BACE2), (2) matrix metalloproteinase (MMP) and insulin degrading enzyme (IDE), and (3) $[Pd(H_2O)_4]^{2+}$ ($I_{MPC}$) and $[Pd_2(\mu\text{-}OH)([18]aneN_6)]^{3+}$ ($\mathbf{I_{DPC}}$). The computed energetics predict that among these catalysts, the $Zn^{2+}$ metal center containing MMP is the most efficient in catalyzing this reaction. The two active site aspartate residues containing BACE2 catalyze this reaction with 5.0 kcal/mol higher barrier than MMP. The substitution of a His ligand with Glu in the metal center of MMP generates the active site of IDE that catalyzes the reaction with a 6.9 kcal/mol higher barrier than MMP. Both artificial peptidases $\mathbf{I_{MPC}}$ and $\mathbf{I_{DPC}}$ catalyze this reaction with significantly high barriers of 35.4 and 31.0 kcal/mol, respectively. The computed energetics of all the catalysts are in line with the available experimental and theoretical data.

## I. Introduction

The selective hydrolytic cleavage of proteins and peptides plays critical functional and regulatory roles in the control of the cell cycle, transcription, signal transduction, antigen processing, and apoptosis.[1,2] This procedure is also common in modern bioengineering applications, such as protein footprinting,[3] proteomics,[1] bioengineering of proteins,[4] bioanalytical analysis,[5] and designing of catalytic drugs.[6−9] These natural and modern processes require the selective cleavage of the specific peptide bond (−(O═)C−NH−), which couples the amino acids in proteins. These bonds are highly stable, and the half-life for the hydrolysis of peptide bonds is 350−500 years at room temperature and pH = 4−8.[10] To accomplish this formidable task, nature has devised highly specialized enzymes, such as aspartyl proteases ($\beta$-secretase (BACE2),[11−14] HIV protease (HIV PR),[15,16] and presenilin 1 (PS1)[17−20]) and metallopeptidases (matrix metalloproteinase (MMP)[21,22] and insulin degrading enzyme (IDE)[23,24]).

In the past few years, several transition metal (Pd, Pt, Zn, Cu, Co, and Fe) complexes have also been synthesized to hydrolyze the amide bond under milder conditions.[6,25−38] In particular, various Pd(II) ion containing metal complexes, such as a mononuclear $[Pd(H_2O)_4]^{2+}$ ($\mathbf{I_{MPC}}$) and dinuclear $[Pd_2(\mu\text{-}OH)([18]ane\text{-}N_6)]^{3+}$, where [18]ane-$N_6$ is 1,4,7,10,13,16-hexaazacyclooctadecane, ($\mathbf{I_{DPC}}$), have been reported to catalyze selective hydrolyses of peptide bonds (where the subscripts MPC and DPC denote the monopalladium complex and dipalladium complex respectively).[33,39−44] However, the hydrolytic reactions promoted by these metal complexes are significantly slower than the ones catalyzed by natural metallopeptidases.[33,25] Thus, a deeper understanding of the precise roles of the microenvironments of the active sites of the current catalysts in peptide hydrolysis can advance our efforts in the designing of more efficient artificial peptidases.[45,46] To enhance this understanding, in the present DFT study, mechanisms of the hydrolysis of a peptide bond (Phe1-Phe2) have been studied by the three different types of catalysts (five in total): (1) aspartyl protease (BACE2, Figure 1a), (2) metallopeptidases (MMP (Figure 1b) and IDE (Figure 1c)), and (3) artificial peptidases ($\mathbf{I_{MPC}}$ (Figure 1d) and $\mathbf{I_{DPC}}$ (Figure 1e)). Both BACE2 and IDE naturally cleave this peptide bond of Alzheimer amyloid beta (A$\beta$) peptides.[11,47−49]

The hydrolytic cleavage of the Phe1-Phe2 bond catalyzed by these catalysts can be represented by the following overall reaction:

$$\text{Phe1}-\text{C}(=\text{O})-\text{N}(-\text{H})-\text{Phe2} + \text{H}_2\text{O} \rightarrow \text{Phe1}-\text{COOH} + \text{Phe2}-\text{NH}_2 \quad (1)$$

$\beta$-Secretase (BACE2), also known as memapsin 1, is an integral membrane aspartyl protease that utilizes the general acid/base mechanism in its catalytic cycle (Figure 2).[11,12,14,50−55] This mechanism has previously been theoretically studied for the other members of the aspartyl protease family, such as HIV protease,[56−60] malaria protease,[61] and presenilin 1 (PS1).[62] In this mechanism, the binding of the substrate at the active site distorts the scissile peptide bond and reduces its double bond character. This polarizes the carbonyl carbon atom to make it susceptible to a nucleophilic attack by the active site water molecule. Here, a catalytic diad formed by one protonated (Asp48) and one unprotonated (Asp241) aspartate residue polarizes the active site water molecule that functions as a powerful nucleophile.[50] In the first step of the mechanism, from reactant (**I**), Asp241 acts as a catalytic base and abstracts a proton from the water molecule, and the hydroxyl (−OH) group nucleophilically attacks the carbonyl carbon atom of the amide bond in a concerted fashion. In this process, the protonated Asp48 functions as an acid by donating its proton to the carbonyl oxygen atom. This step leads to the generation of a transient *gem-diol* intermediate (**II**). In the final step, Asp241 switches its role to an acid and donates the proton to the nitrogen (N) atom of the amide group with the simultaneous abstraction of the proton from the hydroxyl group by Asp48 that now acts as

* To whom correspondence should be addressed. Phone: 305-284-9372. Fax: 305-284-4571. Email: rpr@miami.edu.

10.1021/jp104294x 
Published on Web 07/29/2010

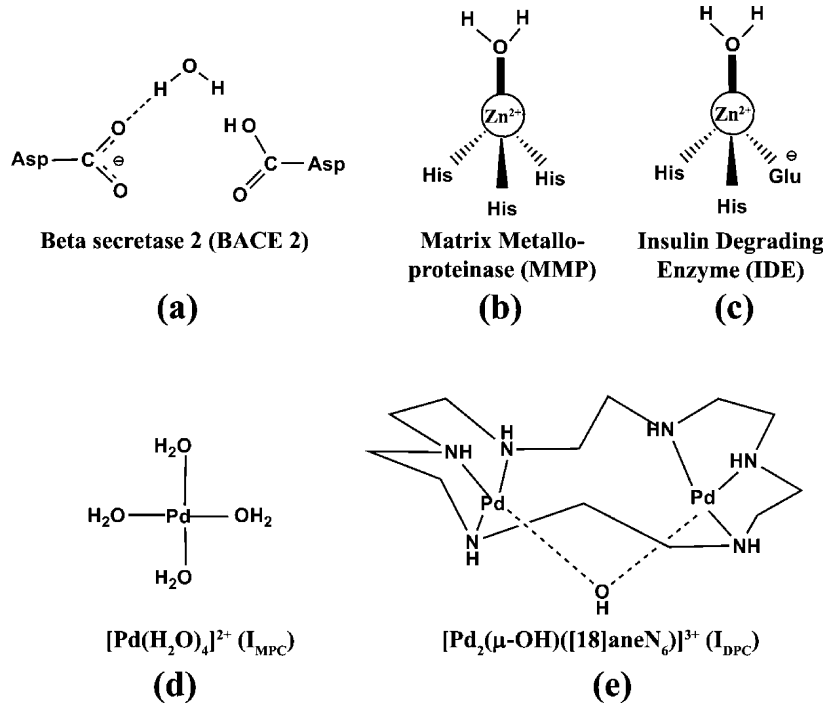


**Figure 1.** Structures of catalysts used in the study.

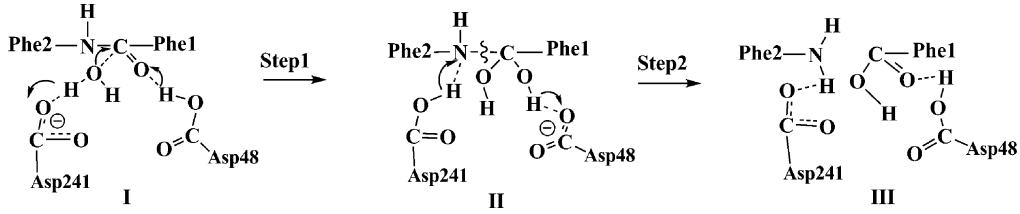


**Figure 2.** Experimentally suggested general acid/base mechanism utilized by aspartyl proteases for peptide hydrolysis. The arrows describe the movement of atoms.

a base. The splitting of the peptide bond in this process creates isolated amine ($-NH_2$) and carboxylic ($-COOH$) products (**III**).

On the other hand, MMP and IDE are the Zn-containing metallopeptidases that catalyze the hydrolysis of a variety of peptide bonds.[21−23,63−66] The Zn metal center of MMP is similar to IDE, except that the $Zn^{2+}$-bound Glu ligand is substituted by a His residue (Figure 1b and 1c). The experimentally proposed general catalytic mechanism utilized by metallopeptidases such as MMP and IDE is shown in Figure 3.[46] This mechanism has previously been theoretically studied for the cleavage of different substrates for MMP,[67,68] IDE,[69,70] and thermolysin (TLN).[71−73] In many aspects, the general mechanism utilized by metallopeptidases in their catalytic cycle is similar to the one used by BACE2 (Figure 2).[46] In the reactant (**I**), the carbonyl oxygen atom ($O^8$) of the substrate interacts with the $Zn^{2+}$ metal ion, whereas in BACE2, it interacts with the protonated Asp48 residue. Here, the metal-bound water molecule ($H^2O^1H^3$) is strongly polarized between the negatively charged Glu and the Zn cation, whereas in BACE2 it is polarized by two aspartate residues. This polarization decreases its p$K_a$ value from ∼14 to ∼7 in solution.[71,74] In the first step, similar to the functioning of Asp241 in BACE2, the second coordination shell Glu residue acts as a base and abstracts a proton from the $Zn^{2+}$ ion-bound water molecule to activate it. The hydroxyl ion ($-O^1H^3$) formed in this process makes a nucleophilic attack on the carbonyl carbon ($C^6$) atom of the peptide bond to generate an intermediate (**II**). In the second step, like Asp241 in BACE2, Glu switches its role to an acid and donates the proton to the $N^7$ atom of the amide group with the simultaneous formation of the oxygen−carbon ($O^1-C^6$) bond. This step leads to the generation of the gem-diol intermediate (**III**). In the final step, similar to Asp48 in BACE2, Glu again functions as a base and pulls the proton ($H^3$) from the metal bound oxygen ($O^1$) atom. As a result of this proton transfer, the $C^6-N^7$ peptide bond is cleaved, and the carboxylate (Phe1$-C^6O^1O^{8-}$) and amine (Phe2$-N^7H_2$) products are generated (**IV**).

The mono- and dinuclear palladium metal center containing artificial proteases $[Pd(H_2O)_4]^{2+}$ ($\mathbf{I_{MPC}}$) and $[Pd_2(\mu\text{-OH})([18]aneN_6)]^{3+}$ ($\mathbf{I_{DPC}}$), respectively, have also been reported to catalyze the cleavage of peptide bonds, (Figure 1d and e). In $\mathbf{I_{MPC}}$, the Pd(II) ion has previously been shown to anchor Met and His residues in X−Y−Met and X−Y−His sequences, respectively, and cleave the proximal X−Y (Gly-Gly, Gly-Pro, and Gly-Sar) peptide bond (Gly = glycine, Pro = proline, and Sar = sarcosine).[25,75] It is noteworthy that $\mathbf{I_{MPC}}$ itself is not the active complex that catalyzes this reaction. The substitution of a metal-bound water molecule by the anchoring Met residue and the subsequent generation and dissociation of a hydronium ion ($H_3O^+$) creates the active bidentate complex (Figure 1 in the Supporting Information).[25,76] The creation of this complex for the Phe1-Phe2-Met sequence used in this study is discussed below. The TOCSY and ROESY $^1$H NMR spectra of the −Gly-Pro-Met−, −Gly-Sar-Met−, −Gly-Gly-Met−, and −Gly-Pro-His− sequences indicate that the active bidentate complex exists in trans conformation.[25] After the creation of this complex, the cleavage of the peptide bond was experimentally proposed to

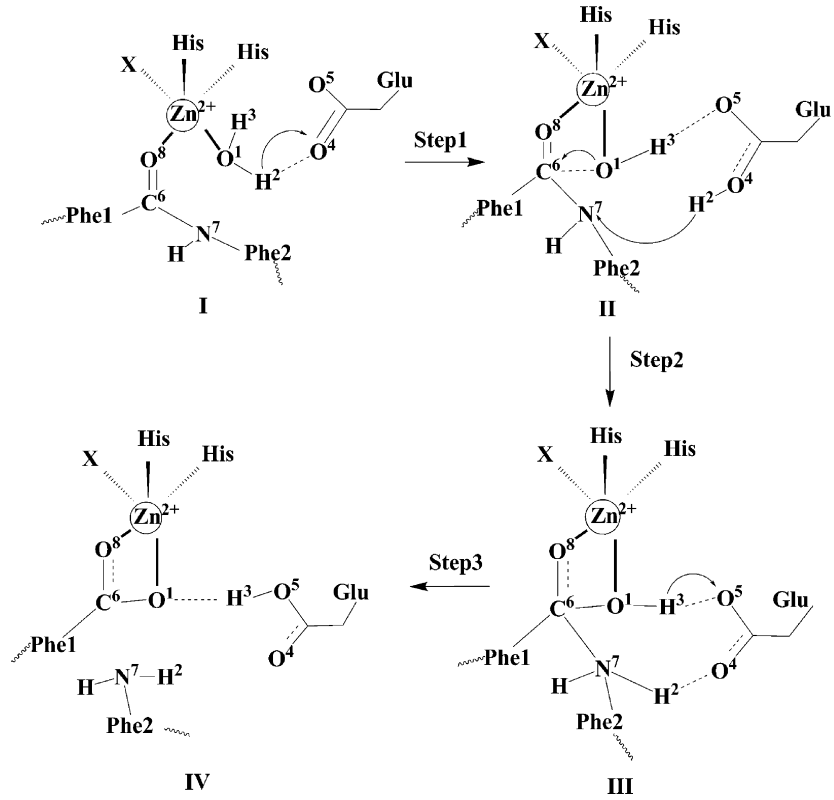


**Figure 3.** Experimentally suggested mechanism utilized by metallopeptidases for peptide hydrolysis (X = His for MMP and X = Glu for IDE). The arrows describe the movement of atoms.

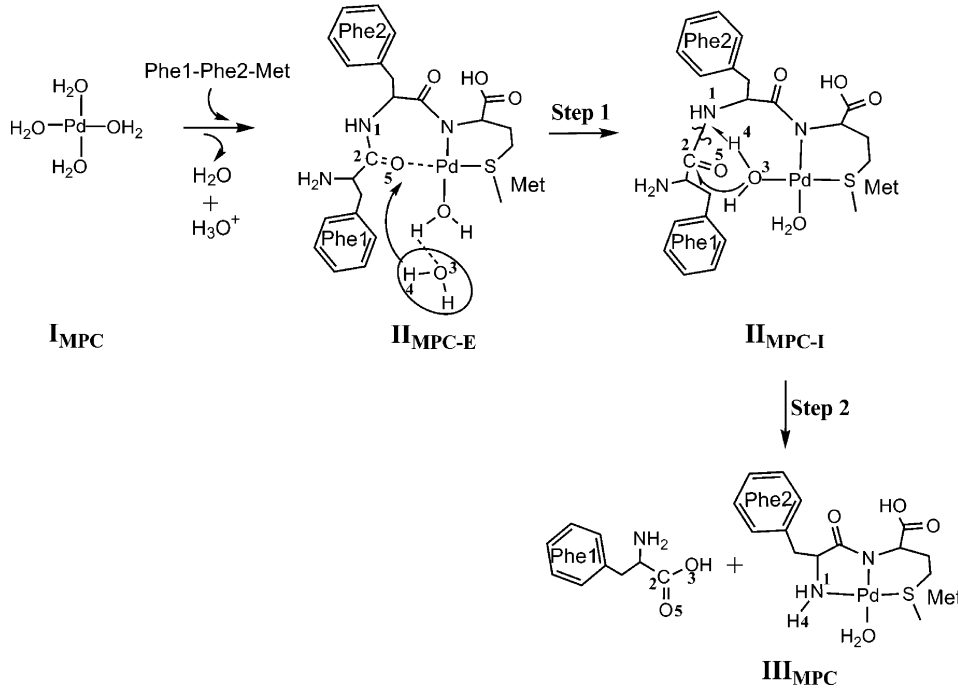


**Figure 4.** Suggested mechanism utilized by $[Pd(H_2O)_4]^{2+}$ for peptide hydrolysis. The arrows describe the movement of atoms.

occur either through an external attack or an internal delivery mechanism of a water molecule (Figure 1 in the Supporting Information).[25]

In a recent B3LYP study, by incorporating available experimental information, the most energetically feasible mechanism for the hydrolysis of Gly-Pro, Gly-Sar, Gly-Gly, and Gly-Pro peptide bonds in the Gly-Pro-Met, Gly-Sar-Met, Gly-Gly-Met, and Gly-Pro-His sequences by $\mathbf{I_{MPC}}$ has been proposed.[76] According to the proposed mechanism, after the formation of the bidentate complex, the internal delivery mechanism is the most plausible for the hydrolysis of the aforementioned peptide bonds.[76]

In this mechanism, the active bidentate complex ($\mathbf{II_{MPC\text{-}E}}$), Figure 4, is generated by the substitution of two metal bound water molecules by the anchoring Met residue and carbonyl group of the scissile peptide bond and the generation and dissociation of a hydronium ion ($H_3O^+$), where subscript -E denotes the presence of a water molecule previously coordinated

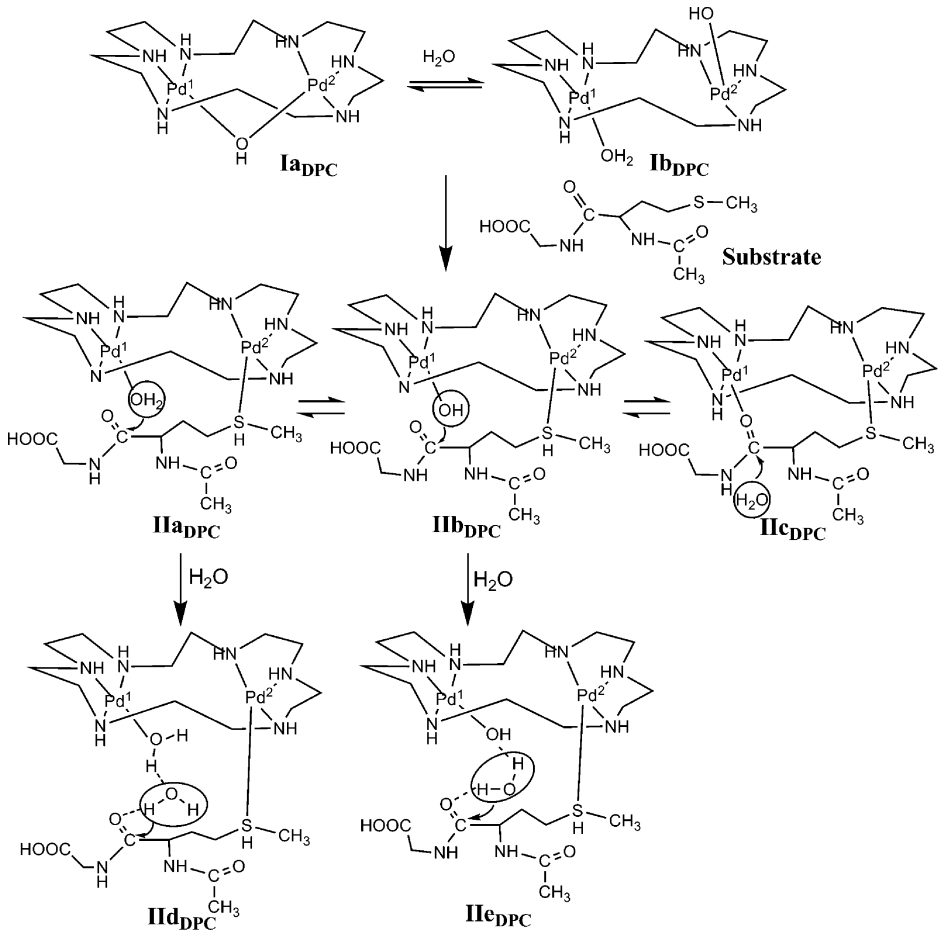


**Figure 5.** Possible mechanisms for peptide hydrolysis utilized by $[Pd_2(\mu\text{-OH})([18]aneN_6)]^{3+}$.

to the Pd ion (circled in Figure 4). In $\mathbf{II_{MPC\text{-}E}}$, the carbonyl atom is oriented toward the Pd(II) ion.[25] In the first step, the reactant $\mathbf{II_{MPC\text{-}E}}$ is transformed to another conformer ($\mathbf{II_{MPC\text{-}I}}$), where subscript -I denotes the structure formed due to the coordination of an external water molecule to the Pd(II) ion (Figure 4). In the next step, the water molecule ($H_2O^3$) bound to the Pd(II) ion in $\mathbf{II_{MPC\text{-}I}}$ is activated. Here, the $O^3-H^4$ bond of the water molecule is broken, and the proton is transferred to the $N^1$ atom of the scissile peptide bond of the substrate. This process occurs concomitant with the transfer of the hydroxyl group ($-O^3H$) to the carbonyl ($C^2$) atom that forms the cleavage site of the substrate and hydrolyzes the peptide bond into separated amine ($-NH_2$) and carboxylic ($-COOH$) groups.

On the other hand, the dinuclear Pd-center-containing complex ($\mathbf{I_{DPC}}$) catalyzes the hydrolysis of an acylated form of a methionine-containing peptide (AcMet-Gly).[33] Electrospray ionization mass spectrometry (ESI-MS) experiments showed that the two dominating species $[Pd_2(\mu\text{-OH})([18]aneN_6)]^{3+}$ ($\mathbf{Ia_{DPC}}$) and $[Pd_2(H_2O)(OH)([18]aneN_6)]^{3+}$ ($\mathbf{Ib_{DPC}}$) exist in an aqueous solution (Figure 5). The substrate was proposed to coordinate to only one metal ion ($Pd^2$) of the dinuclear metal center via the side chain of the methionine residue to form the active complex and hydrolyze the peptide bond.[33] The cleavage of this peptide can occur through the following mechanisms: (1) cleavage through a metal ($Pd^1$)-bound water molecule ($\mathbf{IIa_{DPC}}$); (2) cleavage through a metal-bound hydroxyl ion ($\mathbf{IIb_{DPC}}$); (3) Lewis acid activation ($\mathbf{IIc_{DPC}}$), in which the binding of $Pd^1$ to the carbonyl oxygen atom increases the electrophilicity of the carbon atom of the peptide bond and activates it for an attack by an external water molecule. The first two mechanisms (mechanisms 1 and 2) can also proceed via the assistance of an external water molecule. This gives rise to the following two additional mechanisms: (4) cleavage by an external water molecule trapped between the substrate and the metal bound water molecule ($\mathbf{IId_{DPC}}$) and (5) cleavage by an external water molecule trapped between the substrate and the metal bound hydroxyl molecule ($\mathbf{IIe_{DPC}}$). A comparison of the computed energetics of all the aforementioned mechanisms through DFT calculations indicate that the hydrolysis of the AcMet-Gly peptide bond through the external water molecule trapped between the substrate and the metal bound water molecule (mechanism 4) is the most energetically feasible (these results will be reported elsewhere).

At the starting point of this mechanism ($\mathbf{III_{DPC}}$ in Figure 6), the external water molecule used for the hydrolysis of the peptide bond interacts with the carboxyl terminal group of the substrate through a hydrogen bond. In the first step, the water molecule repositions itself close to the cleavage site and extracts a proton from the metal bound water molecule to generate a hydronium ion ($\mathbf{IV_{DPC}}$, Figure 6). In the next and final step, the hydronium ion in $\mathbf{IV_{DPC}}$ donates a proton and the hydroxyl ion to the nitrogen and carbon atoms of the scissile peptide bond, respectively, and the remaining proton is transferred back to the metal-bound hydroxyl ion. This concerted process leads to the cleavage of the peptide bond and regeneration of the catalyst ($\mathbf{V_{DPC}}$).

The primary objective of this study is to investigate mechanisms of the cleavage of the Phe1-Phe2 peptide bond by a variety of natural (BACE2, MMP and IDE) and artificial ($[Pd(H_2O)_4]^{2+}$ and $[Pd_2(\mu\text{-OH})([18]aneN_6)]^{3+}$) peptidases. The

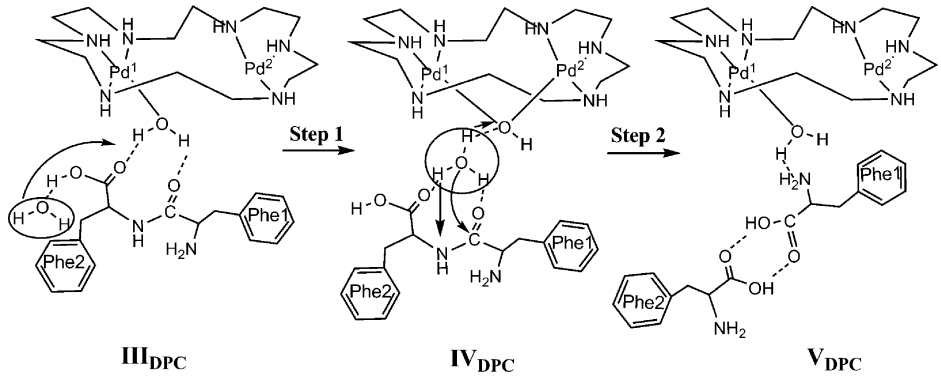


**Figure 6.** The investigated mechanism for peptide hydrolysis utilized by $[Pd_2(\mu\text{-OH})([18]aneN_6)]^{3+}$.

results obtained from this study will allow us to make several interesting comparisons concerning mechanisms and energetics of these reactions: (1) the effect of the active site in an aspartyl protease (BACE2) and metallopeptidases (MMP and IDE), (2) the influence of the ligand environment of the $Zn^{2+}$ center in MMP and IDE, (3) the impact of the nature of the metal center in natural mononuclear $Zn^{2+}$-containing metallopeptidases (MMP and IDE) and artificial mononuclear $Pd^{2+}$-containing metallopeptidase ($\mathbf{I_{MPC}}$), and (4) the effect of the nature and number of the Pd metal centers in mononuclear ($\mathbf{I_{MPC}}$) and dinuclear ($\mathbf{I_{DPC}}$) artificial metallopeptidases. These calculations will provide accurate energetics and structures of all short-lived intermediates and transition states and systematically exhibit how the active site environment, ligand substitution and nature and number of the metal centers determine the kinetics of the peptide hydrolysis.

## II. Computational Procedure

**IIa. Computational Modeling.** A model of the BACE2−substrate (Phe1-Phe2) complex for the DFT calculations was developed through superimposing the X-ray structure of BACE2 with the cocrystal structure of another $\beta$-secretase (BACE1) that exhibits 43% identity and 59% sequence similarity,[13] and MD simulation method. The inhibitor bound X-ray structures of BACE1 (PDB: 1FKN)[78] and BACE2 (PDB: 2EWY)[13] were utilized in constructing the initial models used in these techniques. In these X-ray structures, a peptidomimetic inhibitor (OM99-2) with the sequence EVNL*−A*AEF (where L* and A* are the modified Leu and Ala residues) is bound to BACE1, whereas hydroxyethylenamine (HEA), a transition state based inhibitor is bound to BACE2. Since HEA is structurally very different from the substrate, it was substituted with the OM99-2 inhibitor, which is similar to the actual substrate, in the X-ray structure of BACE2 (PDB ID: 2EWY). The computed root-mean-square deviation (rmsd) between these two structures is only 0.96 Å. On the basis of the spatial occupancy of the backbone atoms of OM99-2 inside BACE2, OM99-2 was converted to the actual substrate (KLVF∼FAED) using the Swiss PDB viewer (SPDBV) program.[79] In accordance with the available experimental and theoretical information, one of the active site aspartates (Asp48) of BACE2 was protonated.[80−82] The initial BACE2−substrate structure was subjected to energy minimization using the AMBER03 module in the YASARA family of programs[83] by keeping the entire enzyme and only the carbonyl oxygen atom of the substrate fixed. This minimization allowed the substrate to reorient itself in an energetically favorable conformation inside the active site of BACE2. In the next step, the resulting BACE2−substrate complex structure was further subjected to an unconstrained 5 ns MD simulation using the GROMACS program[84,85] with the GROMOS force field 53A5.[86] The details of the MD simulations[83−85,86−92] are provided in the Supporting Information.

The root-mean-square deviation (rmsd) of the trajectory indicates that this structure gets equilibrated only after 2 ns, and in the thermodynamically equilibrated region, the overall rmsd remains within a 0.20 nm range (Figure 2a of the Supporting Information). The most representative structure obtained from the 5 ns BACE2−substrate simulation has been used to create the starting model for the DFT calculations (Figure 2b of the Supporting Information). The truncated model for the active site of BACE2 includes Asp48 and Asp241 residues and a conserved water molecule, whereas a tetra peptide (Val-Phe-Phe-Ala) has been utilized as a model for the substrate. The DFT model derived here contains 87 atoms for the BACE2−substrate complex and represents the common structural features of the active site of BACE2. This kind of modeling has been widely used in quantum chemical studies.[62,93−96] To retain the strain of the surrounding enzyme on the active site, the atoms leading to the backbones of Asp residues were kept fixed from the equilibrated structure derived from MD simulations (shown by the asterisk sign in Figure 7). The overall charge of the system is −1 and it exists in the singlet ground state.

The starting model for the IDE−substrate complex is derived from the X-ray structures of the substrate-bound (A$\beta$40) human IDE (PDB ID: 2G47)[23] and the substrate free human IDE (PDB ID: 2JG4).[24] In the substrate-bound structure, the catalytically active Glu residue in the second coordination shell was mutated to Gln, and the $Zn^{2+}$ ion was removed. These substitutions rendered the enzyme in the inactive form. This structure contains only small fragments (Gln3-Arg5, Lys16-Ala21, and Asp23) of the A$\beta$40 substrate, and the Phe19-Phe20 cleavage site is ideally located adjacent to the $Zn^{2+}$ metal center. The substrate-free and the A$\beta$40-bound structures superimpose well with each other (rmsd = 0.18 Å).[24] The starting structure for the DFT calculations was obtained by superimposing both the X-ray structures (2G47 and 2JG4), and during their translation and rotation, the rmsd between them was kept to a minimum. Since the X-ray structure of the substrate-bound MMP is not available, the substrate-bound structure of IDE (PDB ID: 2G47)[23] is used to prepare models of this enzyme. The first coordination shell residue Glu189 of IDE is replaced with the His residue to mimic the active site environment of MMP. Like BACE2 enzyme, the tetra-peptide (Val-Phe-Phe-Ala) substrate was used for the IDE and MMP enzymes. The total charge of the model of IDE and MMP is 0 and +1, respectively, and they both exist in the singlet ground states.

The starting structure for the substrate-bound $[Pd(H_2O)_4]^{2+}$ ($\mathbf{I_{MPC}}$) complex is built based on the available experimental and

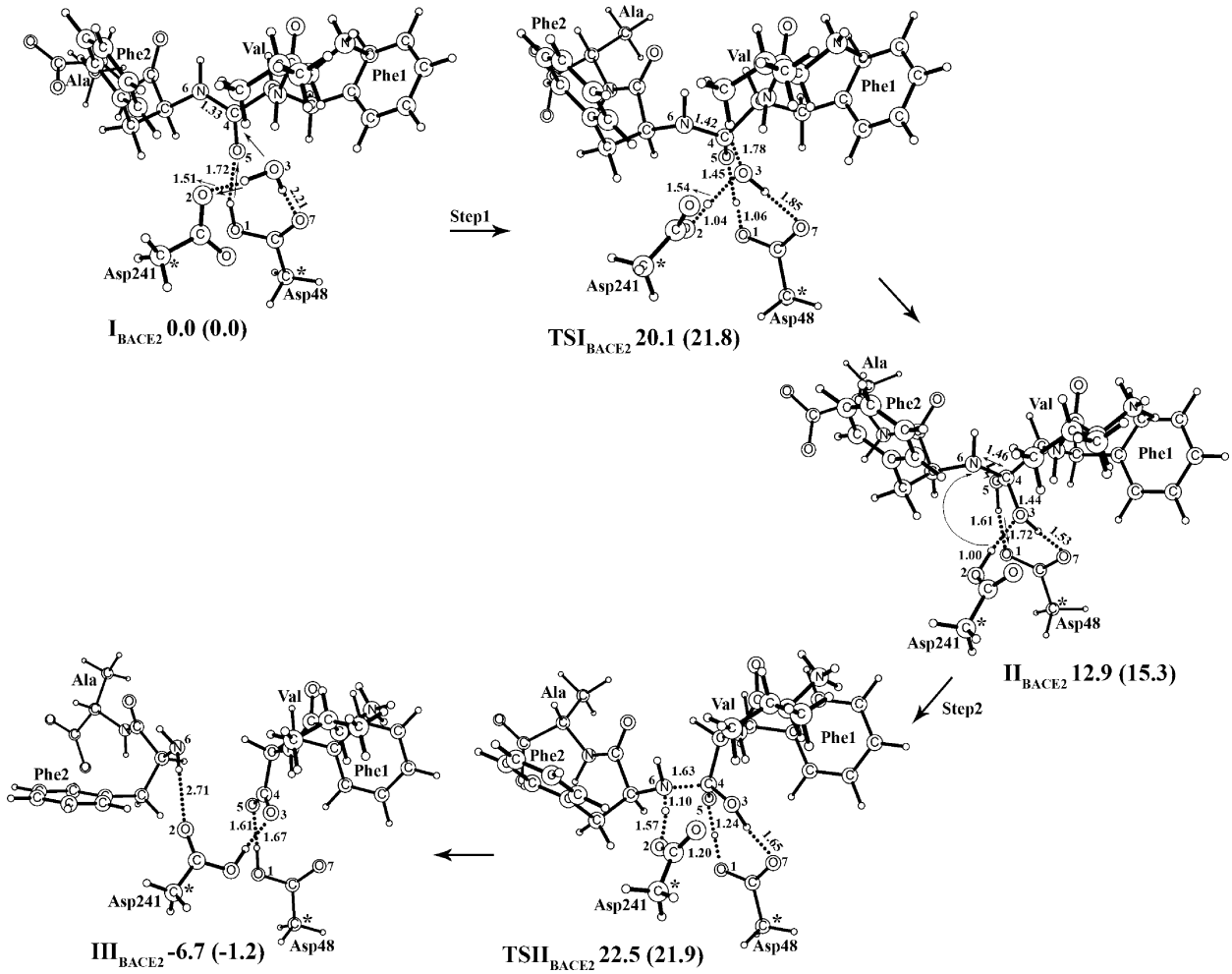


**Figure 7.** Structures (in Å) and energies (in kcal/mol) of the reactant, intermediate, transition states (optimized), and the product for peptide hydrolysis catalyzed by BACE2. Stars indicate the atoms fixed to their equilibrated positions during optimizations.

theoretical information.[76] In the $\mathbf{I_{MPC}}$−substrate complex, a tripeptide (Phe1-Phe2-Met) model of the substrate including anchoring (Met) and the peptide-bond-donating amino acid residues (Phe1-Phe2) was utilized. The starting model for the $\mathbf{I_{DPC}}$ complex is constructed from the X-ray structure (CCDC ID: 253854).[33] In this structure, the two palladium ions are tetracoordinated to three nitrogen atoms and one bridging hydroxo group. The net charge on the starting structures in the $\mathbf{I_{MPC}}$ and $\mathbf{I_{DPC}}$ catalyzed reactions are +1 and +4, respectively, and they also exist in the singlet ground state.

In the models of the active site for BACE2, MMP, and IDE, the His residue was modeled as the imidazole, and Glu and Asp, as the acetate ion. However, the backbones of both constituents of the substrate (Phe1 and Phe2) in all the models and of the anchoring Met residue (only for $\mathbf{I_{MPC}}$) were included.

**IIb. Computational Details.** All calculations were performed using the Gaussian-03 program package.[97] The geometries were optimized without any symmetry constraints using the B3LYP functional.[98−100] For BACE2 (an aspartyl protease) optimizations were performed using the all-electron 6-31G(d) basis set, and for all the metal-containing systems (MMP, IDE, $\mathbf{I_{MPC}}$ and $\mathbf{I_{DPC}}$), the Lanl2dz basis set that includes the Hay−Wadt effective core potential (ECP) for Zn and Pd was utilized.[101] An additional d polarization function for the S atom ($\alpha = 0.55$) was used for the $\mathbf{I_{MPC}}$ complex. The final energies of the optimized structures of BACE2, MMP, and IDE were further improved by performing single point calculations using the 6-311+G(d, p) basis set of the triple-$\zeta$ quality, whereas for $\mathbf{I_{MPC}}$ and $\mathbf{I_{DPC}}$ including additional d and p polarization functions for O ($\alpha = 0.96$), N ($\alpha = 0.74$), C ($\alpha = 0.59$), and H ($\alpha = 0.36$) atoms, respectively (taken from the EMSL's Gaussian basis set library), in the basis set was used for optimizations. Hessians were calculated at the corresponding levels of theory as the optimizations to confirm the nature of the stationary points along the reaction coordinate. The transition states were confirmed to have only one negative eigenvalue corresponding to the reaction coordinates. The dielectric constants of 4.3 (for BACE2, MMP, and IDE) and 78.39 (for $\mathbf{I_{MPC}}$ and $\mathbf{I_{DPC}}$) corresponding to diethylether and water, respectively, were used to estimate the effect of the surrounding environment utilizing the self-consistent reaction field IEFPCM method.[102] Since, to retain the steric effect of the surrounding protein, some of the backbone atoms were constrained in BACE2, MMP, and IDE, the zero-point vibrational and entropy effects were not included for these systems. Throughout the manuscript, the energies obtained at the B3LYP/6-311+G(d,p) + solvent effects in protein for BACE2, MMP, and IDE and B3LYP/{Lanl2dz + d(S, O) + p(H)} + zero-point energy (unscaled) + thermal and entropy corrections (at 298.15 K and 1 atm) + solvent effects in water for $\mathbf{I_{MPC}}$ and $\mathbf{I_{DPC}}$ are discussed. For all the systems, the energies without solvent effects are provided in parentheses.

## III. Results and Discussion

The reaction 1 is computed to be endothermic by 7.1 (1.5) kcal/mol. In the manuscript, first the hydrolysis of the Phe1-

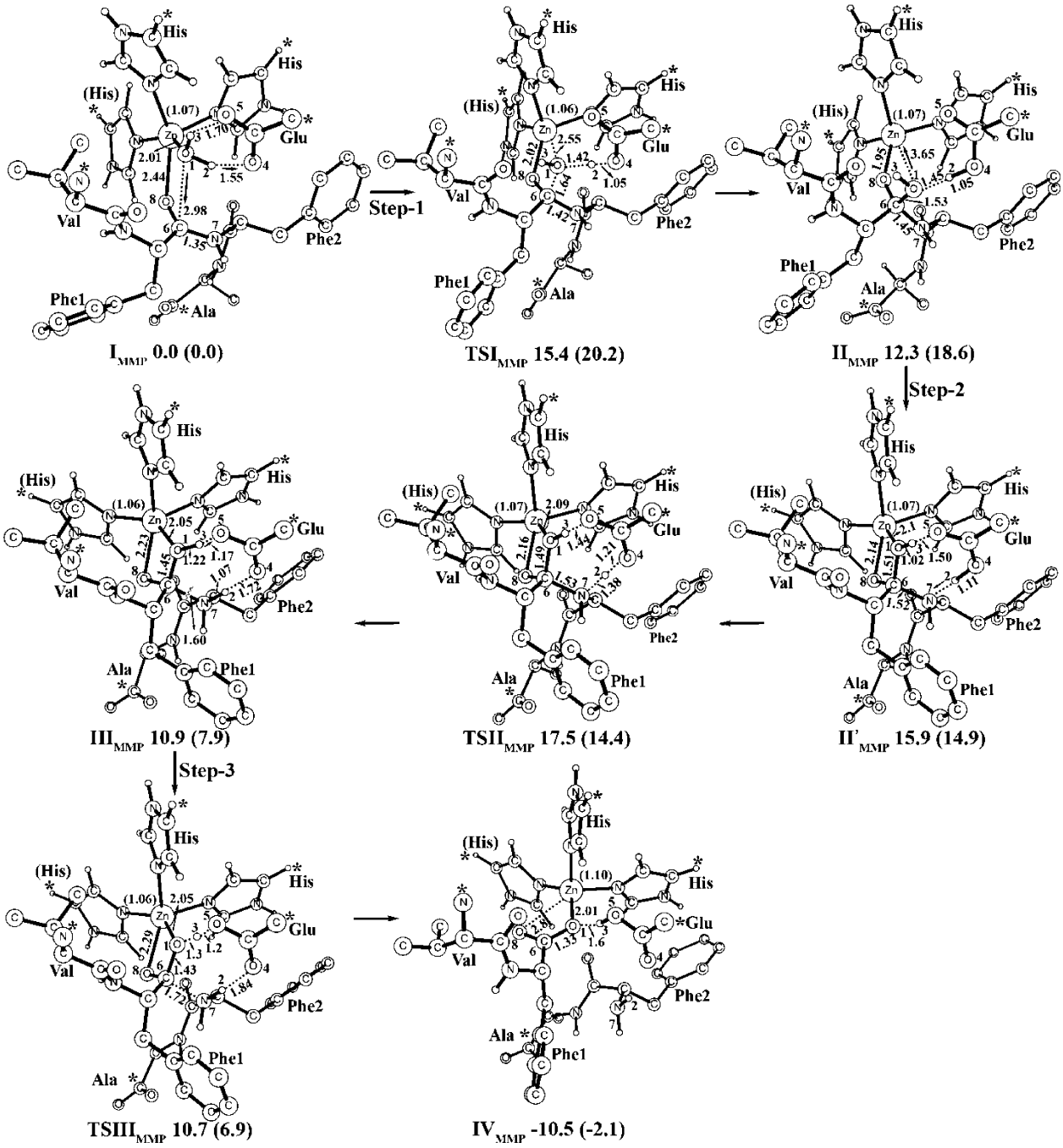


**Figure 8.** Structures (in Å) and energies (in kcal/mol) of the reactant, intermediates, and transition states (optimized) and the product for peptide hydrolysis catalyzed by MMP. Stars indicate the atoms fixed to their crystallographic positions during optimizations and the noncritical hydrogen atoms have been omitted in the figure. The arrows describe the movement of atoms, and the charge on the Zn(II) ion is shown in parentheses. The His residue in parentheses is replaced by Glu in IDE.

Phe2 bond by BACE2 is discussed, followed by its cleavage through MMP, IDE, $\mathbf{I_{MPC}}$, and $\mathbf{I_{DPC}}$.

**IIIa. Hydrolysis of Phe1-Phe2 Bond by $\beta$-Secretase.** In the most representative structure extracted from the 5 ns MD simulation of the BACE2−substrate complex, the catalytic triad (Asp48−$H_2O$−Asp241) is ideally located next to the highly hydrophobic peptide bond cleavage site formed by Phe1-Phe2 (Figure 2b in the Supporting Information). The cleavage of the Phe1-Phe2 peptide bond occurs through the following two steps: (1) formation of the gem-diol intermediate and (2) cleavage of the peptide bond.

***IIIa1. Formation of the Gem-Diol Intermediate.*** In the optimized structure of the reactant ($\mathbf{I_{BACE2}}$), the active site water molecule forms a network of hydrogen bonds with Asp48, Asp241 and the backbone carbonyl oxygen atom ($O^5$) of the Phe1 residue of the substrate ($O^2-H = 1.51$, $O^3H-O^7 = 2.21$, and $O^5-H = 1.72$ Å), Figure 7. From $\mathbf{I_{BACE2}}$, the unprotonated Asp241 acts as a base and abstracts a proton from the active site water molecule ($H_2O^3$) to create the hydroxyl ion ($O^3H^-$). The $-O^3H$ ion created in this process immediately makes a nucleophilic attack at the carbon atom ($C^4$) of the scissile bond concomitantly with the proton transfer from Asp48 to the carbonyl oxygen ($O^5$) atom. In this process, Asp48 plays the role of an acid by donating a proton. In the fully optimized transition state structure ($\mathbf{TSI_{BACE2}}$) of this step, all the relevant bond distances ($O^2-H = 1.04$, $O^3-H = 1.54$, $O^3-C^4 = 1.78$, $O^1-H = 1.06$, and $O^5-H = 1.45$ Å) indicate that this process is synchronous (Figure 7). The computed barrier for this process

**TABLE 1: A Comparison between the Rate-Limiting Barriers for All the Catalysts**

| catalyst | barrier (kcal/mol) |
|---|---|
| MMP | 0.0 |
| BACE2 | +5.0 |
| IDE | +6.9 |
| $[Pd_2([18]aneN_a)]^{4+}$ | +13.5 |
| $[Pd(H_2O)_4]^{2+}$ | +17.9 |

is 20.1 (21.8) kcal/mol. This barrier is in excellent agreement with the measured barrier of ~18 kcal/mol for another member of the human aspartyl protease family BACE1 or memapsin 2.[55] The activation of $H_2O^3$ in this process leads to the creation of the gem-diol intermediate ($\mathbf{II_{BACE2}}$) in which two hydroxyl groups ($O^3H$ and $O^5H$) are attached to the $C^4$ atom of the peptide bond (Figure 7). In $\mathbf{II_{BACE2}}$, the two hydroxyl groups interact with Asp48 through two strong hydrogen bonds ($O^5H-O^1 = 1.61$ and $O^3H-O^7 = 1.53$ Å) and with Asp241 via an additional hydrogen bond ($O^2H-O^3 = 1.72$ Å). The generation of $\mathbf{II_{BACE2}}$ is endothermic by 12.9 (15.3) kcal/mol from $\mathbf{I_{BACE2}}$, and the protonation states of Asp48 and Asp241 are now interchanged, that is, the former is unprotonated, while the latter becomes protonated. In a previous study concerning the cleavage of the Val-Ile and Ala-Thr peptide bonds by presenilin 1 (PS1), the formation of the gem-diol intermediate was also computed to be endothermic by 6.2 and 17.4 kcal/mol, respectively.[62]

***IIIa2. Cleavage of the Peptide Bond.*** Here, the roles played by Asp48 and Asp241 residues are reversed from the previous step. From $\mathbf{II_{BACE2}}$, the Asp241 residue, which acted as a base initially and was protonated during the first step, now acts as an acid and donates its previously acquired proton to the nitrogen ($N^6$) atom of the Phe1-Phe2 cleavage site. This event occurs concurrent to the abstraction of a proton bound to the $O^5$ atom of the gem-diol species by Asp48. The entire process is accompanied by the following significant rearrangement within the active site environment: (1) From $\mathbf{II_{BACE2}}$, the side chain of Asp241 flips 90° and positions itself within the optimal distance to participate in the catalytic activity, and (2) the side chain of Phe2 bends to facilitate the proton transfer from Asp241 to the $N^6$ atom of the peptide bond ($N^6-C^4$). It is worth mentioning that all the aforementioned rearrangements occur themselves during the optimization. This double proton exchange results in the splitting of the Phe1-Phe2 bond. From $\mathbf{II_{BACE2}}$, the computed barrier for this step is 9.6 (6.6) kcal/mol. Since this step is followed by a step that is endothermic by 12.9 (15.3) kcal/mol, the overall barrier for this process becomes 22.5 (21.9) kcal/mol from $\mathbf{I_{BACE2}}$. This step was found to be rate-limiting in the entire mechanism. However, in the cleavage of the Val4-Ile5 and Ala4-Thr5 bonds in Gly1-Gly2-Val3-Val4-Ile5-Ala6-Thr7-Val8 and Val1-Val2-Ile3-Ala4-Thr5-Val6-Ile7-Val8 sequences, respectively, by PS1, the creation of the gem-diol intermediate was computed to occur in the rate-determining

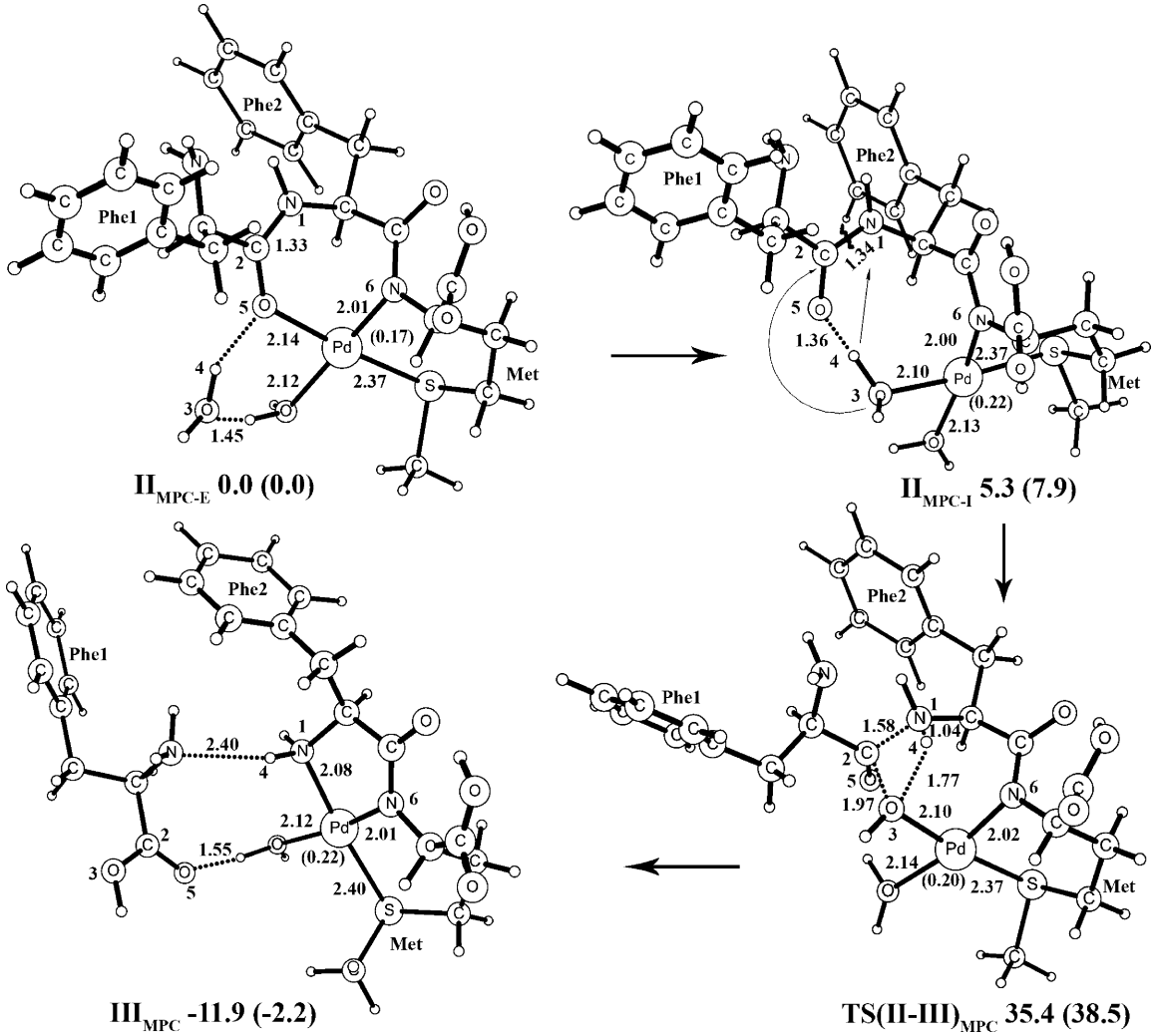


**Figure 9.** Structures (in Å) and energies (in kcal/mol) of the reactant, intermediate, transition state (optimized), and the product for peptide hydrolysis catalyzed by $[Pd(H_2O)_4]^{2+}$. The arrows describe the movement of atoms, and the charge on the Pd(II) ion is shown in parentheses.

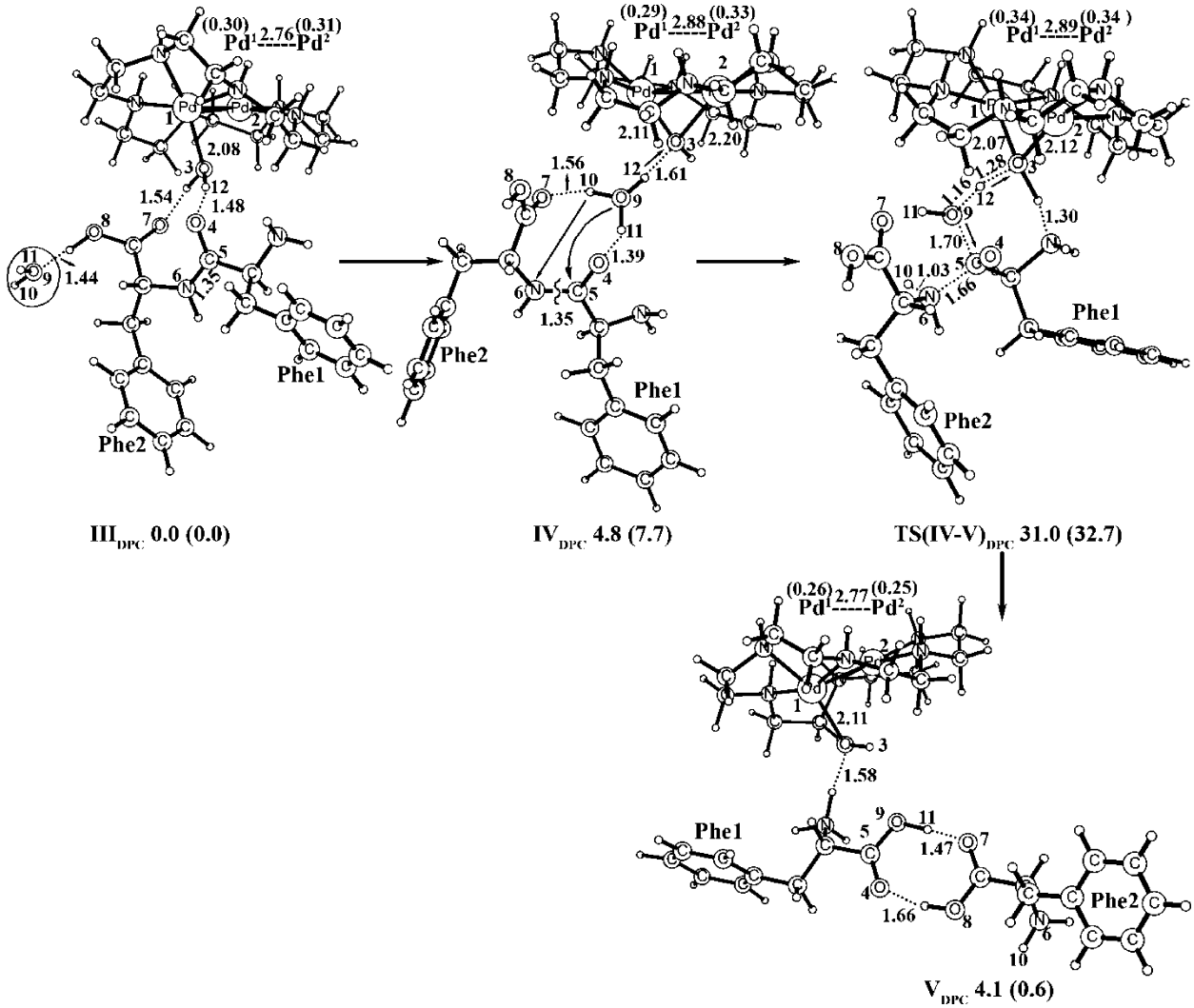


**Figure 10.** Structures (in Å) and energies (in kcal/mol) of the reactant, intermediate, transition state (optimized), and the product for peptide hydrolysis catalyzed by $[Pd_2(\mu\text{-OH})([18]aneN_6)]^{3+}$. The arrows describe the movement of atoms, and the charges on the Pd(II) ions are shown in parentheses.

step.[62] These results are supported by an experimental observation that the nature of the P2′ residue (one amino acid residue downstream from the cleavage site) of the substrate can influence the cleavage mechanisms.[103] Furthermore, the barrier for this process is in line with the measured barrier of ∼18 kcal/mol for memapsin 2.[55] The fully optimized transition state (**TSII$_{BACE2}$**) for this process is shown in Figure 7. The $O^2-H = 1.57$, $N^6-H = 1.10$, $C^4-N^6 = 1.63$, $O^5-H = 1.24$, and $O^1-H = 1.20$ Å bond distances indicate that this process is concerted. From **I$_{BACE2}$**, the hydrolysis of the Phe1-Phe2 peptide bond leading to the formation of Phe1$-COO^-$ and Phe2$-NH_2$ products (**III$_{BACE2}$**) is exothermic by 6.7 (1.2) kcal/mol.

**IIIb. Hydrolysis of the Phe1-Phe2 Peptide Bond by Metalloproteinase (MMP) and Insulin Degrading Enzyme (IDE).** The hydrolysis of the Phe1-Phe2 peptide bond by the $Zn^{2+}$-containing MMP and IDE metallopeptidases proceeds through the following three steps: (1) activation of the metal-bound water molecule, (2) formation of the gem-diol intermediate, and (3) cleavage of the peptide bond. In addition, a concerted mechanism that after the first step directly leads to the cleavage of the peptide bond has been investigated. In this section, first the catalytic mechanism of MMP is discussed, followed by a comparison with IDE and BACE2.

***IIIb1. Activation of the Metal-Bound Water Molecule.*** At the starting point of the mechanism of MMP, the carbonyl oxygen atom ($O^8$) of the Phe1 residue of the substrate interacts with the $Zn^{2+}$ metal center ($Zn-O^8 = 2.44$ Å) to form the active enzyme−substrate complex (**I$_{MMP}$**) (Figure 8). In **I$_{MMP}$**, the active site water molecule ($H^2O^1H^3$) is bound to the $Zn^{2+}$ ion ($Zn-O^1 = 2.01$ Å) and forms two strong hydrogen bonds with the second coordination shell Glu residue ($O^1H^2-O^4 = 1.55$ and $O^1H^3-O^5 = 1.70$ Å) (Figure 8). The substitution of His (shown in parentheses in Figure 8) with a negatively charged Glu that creates the $Zn^{2+}$ metal center of IDE significantly alters these bond distances. In the reactant of IDE (**I$_{IDE}$**), in comparison with **I$_{MMP}$**, the $Zn-O^8$ bond distance shrinks by 0.29 Å and $Zn-O^1$ elongates by 0.10 Å (Figure 3 in the Supporting Information). The $O^1H^2-O^4$ and $O^1H^3-O^5$ bond distances also increase and decrease by 0.94 and 0.34 Å, respectively. However, the charge on the Zn atom in **I$_{MMP}$** is only 0.02*e* lower than in **I$_{IDE}$**. The charges on the other key atoms in both these structures are also quite similar.

In the first step of the mechanism, Glu plays the role of a base by accepting the proton ($H^2$) from the metal bound water molecule ($H^2O^1H^3$). The hydroxyl group ($-O^1H^3$) formed in this process concomitantly makes a nucleophilic attack to the carbon atom ($C^6$) of the scissile peptide bond ($C^6-N^7$, Figure 8). The approach of the $-O^1H^3$ group to the $C^6$ atom is accompanied by the shortening of the bond between the $O^8$ atom of the carbonyl group and the $Zn^{2+}$ ion. The computed barrier

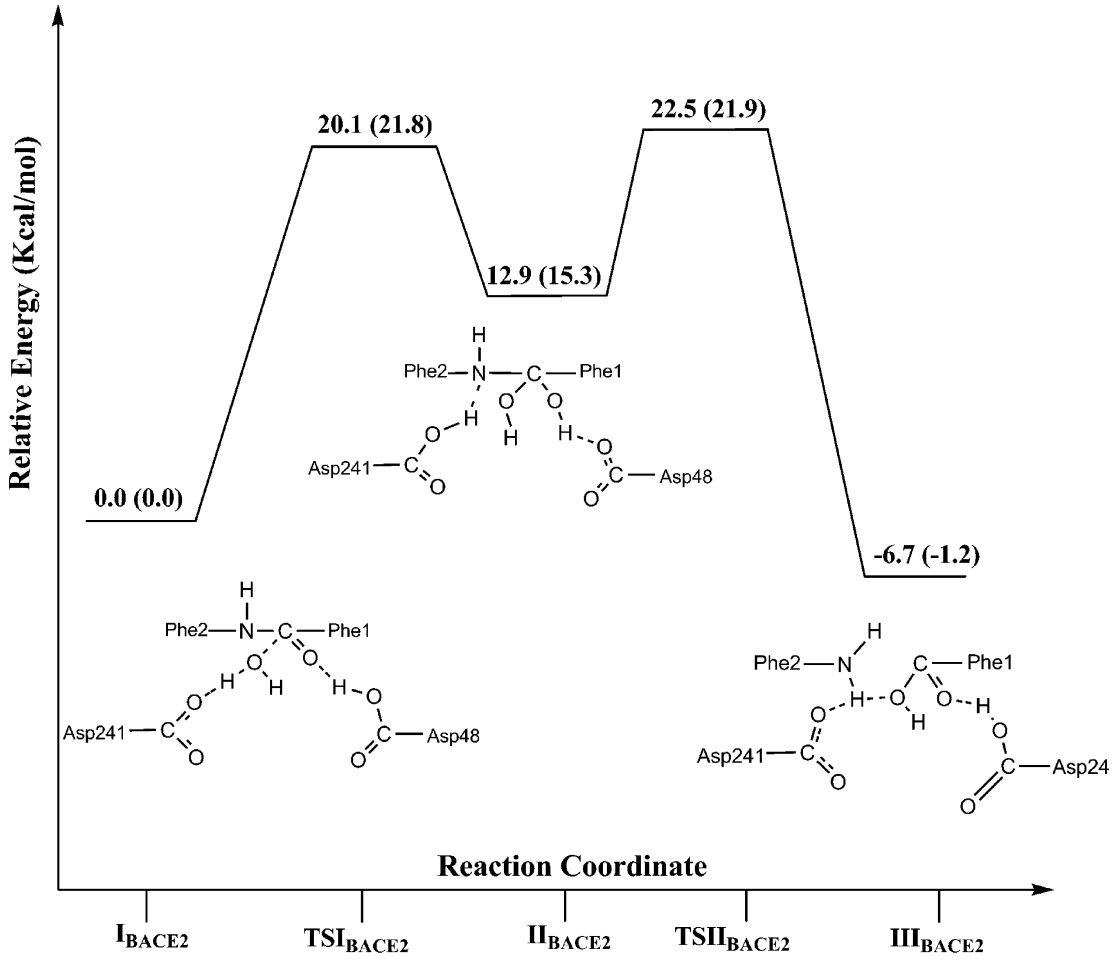


**Figure 11.** Potential energy diagram for peptide hydrolysis catalyzed by BACE2.

for this concerted process is 15.4 (20.2) kcal/mol, and the optimized transition state ($\mathbf{TSI_{MMP}}$) is shown in Figure 8. However, for IDE, the barrier for this step is substantially higher by 9.0 (5.2) kcal/mol; that is, 24.4 kcal/mol from the reactant ($\mathbf{I_{IDE}}$). The main reason for this difference may be the aforementioned structural differences between $\mathbf{I_{MMP}}$ and $\mathbf{I_{IDE}}$. This information can be used in designing artificial peptidases for the degradation of Alzheimer amyloid beta peptide. Moreover, the barrier for IDE is also 5.6 (8.8) kcal/mol higher than the one calculated using a smaller dipeptide model of the substrate in our previous B3LYP study.[69] The reason for this increase in the barrier could be the significantly shorter (by 0.04 Å) bond length of the scissile peptide bond in the optimized transition state ($\mathbf{TSI_{IDE}}$) using the tetrapeptide model of the substrate than the dipeptide one. Furthermore, in TLN also, this step was proposed to be the rate-limiting step,[71] and both the experimentally measured (12.4−16.3 kcal/mol)[104] and calculated (15.2 kcal/mol)[71] values for this process are quite close to the barrier for MMP.

Between MMP and IDE, this step, rather surprisingly, was found to be the rate-limiting process only in the catalytic cycle of IDE. This result indicates that the substitution of Glu with His in the $Zn^{2+}$ metal center exerts a profound effect on the mechanism of IDE by shifting the rate-determining step. On the other hand, for the two active site aspartate residues (protonated Asp48 and unprotonated Asp241) containing BACE2, the computed barrier for the water activation process is higher by 4.7 kcal/mol than MMP and 4.3 kcal/mol lower than IDE. In the optimized transition state for MMP ($\mathbf{TSI_{MMP}}$), in comparison with $\mathbf{TSI_{IDE}}$, the key bond distances are quite different; that is, $O^1-H^2$ and $Zn-O^8$ are longer by 0.01 and 0.08 Å, respectively, whereas $Zn-O^1$, $H^2-O^4$, and $O^1-C^6$ are shorter by 0.27, 0.03, and 0.06 Å, respectively. In the product ($\mathbf{II_{MMP}}$) of this step, Glu is in the protonated form and the $-O^1H^3$ hydroxyl group is coordinated to the $C^6$ atom. The formation of $\mathbf{II_{MMP}}$ is endothermic by 12.3 (18.6) kcal/mol, which is 4.3 kcal/mol lower than the generation of $\mathbf{II_{IDE}}$. However, in contrast to $\mathbf{II_{MMP}}$, $\mathbf{II_{IDE}}$ adopts a different conformation in which protonated Glu is oriented toward the peptide bond cleavage site (Figure 3 in the Supporting Information).

***IIIb2. Formation of the Gem-Diol Intermediate.*** In the second step of the mechanism, the protonated Glu in $\mathbf{II_{MMP}}$ now plays the role of an acid and delivers the proton it previously accepted from the metal bound water molecule to the $N^7$ atom of the $C^6-N^7$ peptide bond. To transfer this proton, the side chain of Glu has to reorient toward the $N^7$ atom. This rotation results in a new intermediate ($\mathbf{II'_{MMP}}$) that lies only 3.6 kcal/mol higher than $\mathbf{II_{MMP}}$ (Figure 8). This rearrangement allows the $O^5$ atom of Glu to form a strong hydrogen bond with the hydroxyl group ($-O^1H^3$) coordinated to the $C^6$ atom ($H^3-O^5$ = 1.50 Å). This process is accompanied by the coordination of the $Zn^{2+}$ ion with the $C^6$ bound hydroxyl ($-O^1H^3$) group ($Zn-O^1$ = 2.10 Å) and the elongation of the $Zn-O^8$ bond distance by 0.19 Å. Furthermore, in comparison with $\mathbf{II_{MMP}}$, the $C^6-N^7$ peptide bond becomes longer by 0.07 Å.

The $\mathbf{II'_{MMP}}$ intermediate is structurally similar to $\mathbf{II_{IDE}}$ created in the previous step. Since this step involves the rotating of a carboxylic group and breaking a hydrogen bond and forming a

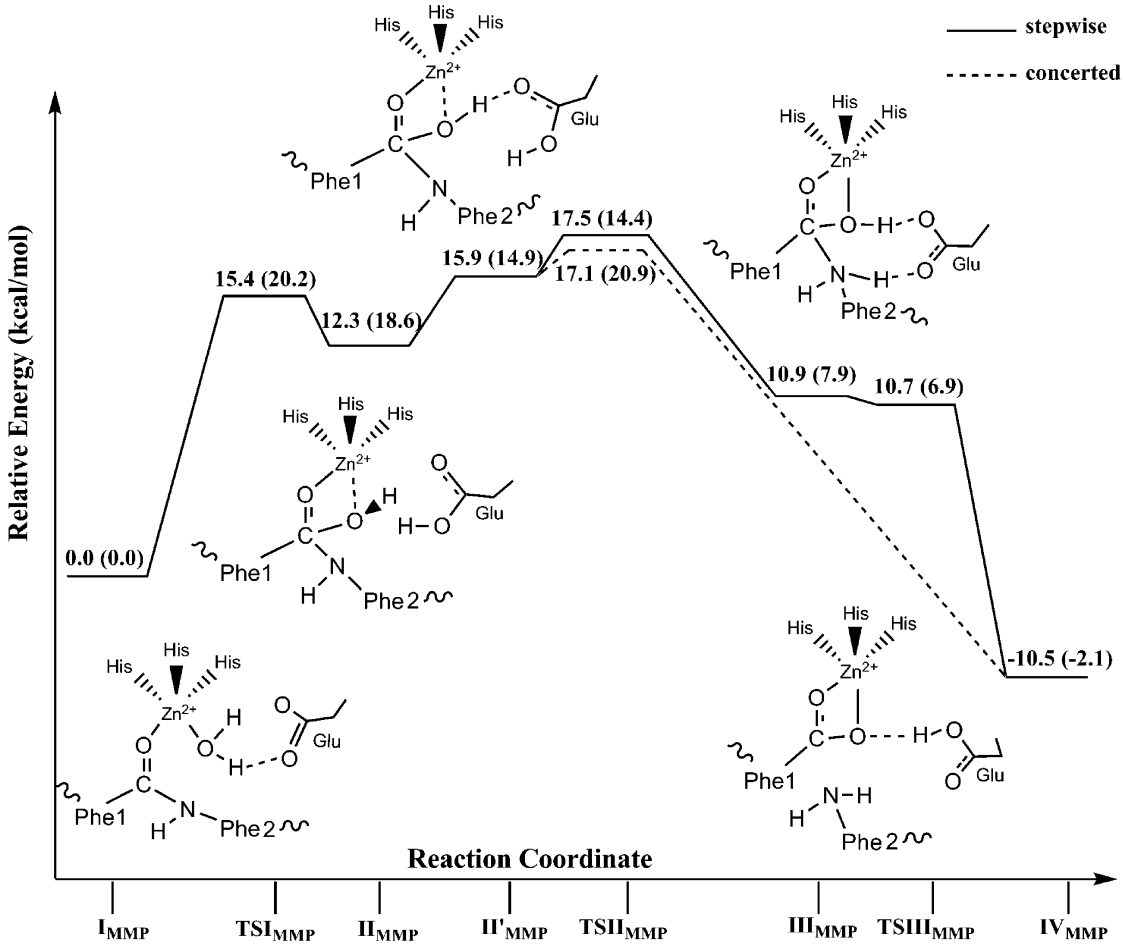


**Figure 12.** Potential energy diagram for peptide hydrolysis catalyzed by MMP.

new one, the transition state for the $\mathbf{II}_{\mathbf{MMP}} \rightarrow \mathbf{II'}_{\mathbf{MMP}}$ transformation could not be located. However, the optimized transition state ($\mathbf{TSII}_{\mathbf{MMP}}$) for the transfer of $H^2$ proton from the optimized Glu to the $N^7$ atom of the peptide bond is depicted in Figure 8. All the critical bond distances in ($\mathbf{TSII}_{\mathbf{MMP}}$) indicate that this process is concerted ($O^4-H^2 = 1.21$ and $N^7-H^2 = 1.38$ Å). This process traverses only a small barrier of 1.60 (−0.5) kcal/mol from $\mathbf{II'}_{\mathbf{MMP}}$. Since this step follows a step that is endothermic by 15.9 (14.9) kcal/mol, the overall barrier for this process from the reactant ($\mathbf{I}_{\mathbf{MMP}}$) becomes 17.5 (14.4) kcal/mol. This is the rate-determining step in the entire mechanism of MMP. In a previous theoretical study on the peptide hydrolysis by MMP, this process was also proposed to be the rate-determining.[105] In IDE also, this process occurs with a similar barrier of 17.8 kcal/mol, but as discussed above, it is not the rate-determining step. The gem-diol intermediate ($\mathbf{III}_{\mathbf{MMP}}$) generated in this step is stabilized by the two strong hydrogen bonds contributed by the Glu residue ($O^4-H^2 = 1.72$, and $O^5-H^3 = 1.17$ Å).

The formation of $\mathbf{III}_{\mathbf{MMP}}$ is endothermic by 10.9 (7.9) kcal/mol from $\mathbf{I}_{\mathbf{MMP}}$. In $\mathbf{III}_{\mathbf{MMP}}$, Glu is in the unprotonated form, and the peptide bond is significantly activated ($C^6-N^7 = 1.60$ Å). However, in IDE, the creation of the gem-diol intermediate is more endothermic by 4.1 kcal/mol; that is, 15.0 kcal/mol higher than $\mathbf{I}_{\mathbf{IDE}}$. These results show that in MMP, this intermediate is more stable than IDE. This could be due to the excess of charge on the $O^1$ (by 0.05 e) and $C^6$ (by 0.08 e) atoms of $\mathbf{III}_{\mathbf{MMP}}$ as compared with their counterparts in $\mathbf{III}_{\mathbf{IDE}}$. However, the charge on the $Zn^{2+}$ atom in both enzymes is quite similar: 1.06*e* for MMP and 1.07*e* for IDE.

***IIIb3. Cleavage of the Peptide Bond.*** In the final step of the mechanism, in a reversal of its role, Glu now acts as a base and abstracts the proton ($H^3$) from the hydroxyl group ($-O^1H^3$) bound to both the $Zn^{2+}$ ion and $C^6$ atom of the gem-diol intermediate ($\mathbf{III}_{\mathbf{MMP}}$, Figure 8). This proton abstraction leads to the concomitant cleavage of the $C^6-N^7$ peptide bond. The optimized transition state ($\mathbf{TSIII}_{\mathbf{MMP}}$) for this process is shown in Figure 8, and the computed barrier for this step was found to be slightly lower, 0.20 (1.00) kcal/mol, than the gem-diol intermediate $\mathbf{III}_{\mathbf{MMP}}$. All the corresponding distances in $\mathbf{TSII\text{-}I}_{\mathbf{MMP}}$ indicate that this process is synchronous ($O^1-H^3 = 1.30$, $O^5-H^3 = 1.20$, and $C^6-N^7 = 1.72$ Å). However, in IDE, the collapse of the gem-diol intermediate ($\mathbf{III}_{\mathbf{IDE}}$) occurs with a small barrier of 2.5 (1.5) kcal/mol. The formation of the separated Phe1−$COO^-$ and Phe2−$NH_2$ products ($\mathbf{IV}_{\mathbf{MMP}}$) is exothermic by 21.4 (10.0) kcal/mol from $\mathbf{III}_{\mathbf{MMP}}$; that is, 10.5 (2.1) kcal/mol exothermic from $\mathbf{I}_{\mathbf{MMP}}$. In $\mathbf{IV}_{\mathbf{MMP}}$, the carboxyl group of Phe1 is bound to the $Zn^{2+}$ ion and Glu is in the protonated form.

In addition, an alternative mechanism for the cleavage of the peptide from $\mathbf{II}_{\mathbf{MMP}}$ directly leading to the generation of $\mathbf{IV}_{\mathbf{MMP}}$ is explored. According to this mechanism, in a concerted manner, the proton $H^2$ from Glu is delivered to the $N^7$ atom with the simultaneous release of a proton from the $C^6$ bound hydroxyl ($-O^1H^3$) group to the $O^5$ atom of Glu (Figure 4 in the Supporting Information). The optimized transition state for this process ($\mathbf{TSII'}_{\mathbf{MMP}}$) is shown in Figure 4 of the Supporting Information, and the barrier for this process is slightly lower (0.38 kcal/mol) than the one computed for the stepwise mechanism discussed above.

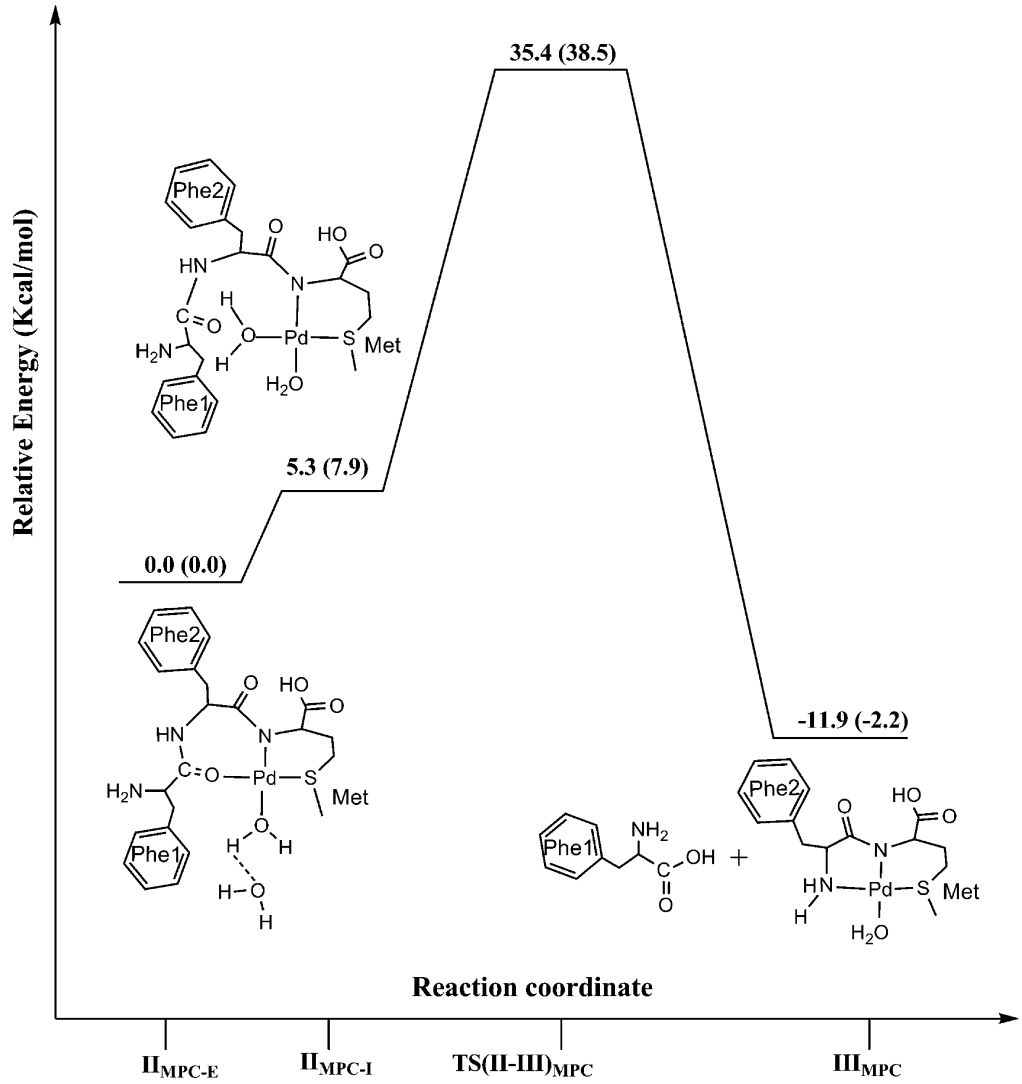


**Figure 13.** Potential energy diagram for peptide hydrolysis catalyzed by $[Pd(H_2O)_4]^{2+}$.

However, the accuracy of the B3LYP in computing the barrier (3−5 kcal/mol) does not allow discrimination between these two mechanisms.

These results show that among BACE2, MMP, and IDE, with the rate-limiting barrier of 17.5 kcal/mol, MMP is the most efficient catalyst in cleaving the Phe1-Phe2 peptide bond, followed by BACE2 and IDE that catalyze this reaction with barriers higher by 5.0 and 6.9 kcal/mol, respectively (Table 1).

**IIIc. Hydrolysis of Phe1-Phe2 Bond by $[Pd(H_2O)_4]^{2+}$ ($\mathbf{I_{MPC}}$) Complex.** As discussed above, in the mechanism of the hydrolysis of the Phe1-Phe2 bond in the Phe1-Phe2-Met peptide by $[Pd(H_2O)_4]^{2+}$ ($\mathbf{I_{MPC}}$), the actual reactive species is the bidentate complex ($\mathbf{II_{MPC-E}}$, Figure 9).[76,25]

In the first step of the mechanism, the reactant $\mathbf{II_{MPC-E}}$ is transformed to the $\mathbf{II_{MPC-I}}$ conformation (Figure 9). The $\mathbf{II_{MPC-E}} \rightarrow \mathbf{II_{MPC-I}}$ transformation is caused by the substitution of the water molecule ($H_2O^3$) and the dissociation of the Pd−$O^5$ bond. Due to the complexity of this transformation, it is not possible to locate the corresponding transition state(s). However, it is not likely to affect the overall mechanism and energetics of this reaction. In comparison with the $\mathbf{II_{MPC-E}}$, the $N^1$−$C^2$ bond is longer by 0.01 Å in $\mathbf{II_{MPC-I}}$, and the charge on the Pd atom is higher by 0.05*e*. In $\mathbf{II_{MPC-I}}$, the $N^1$−$C^2$, Pd−$O^3$, and Pd−$N^6$ bond distances are 1.34, 2.10, and 2.00 Å, respectively, and it is computed to be 5.3 (7.9) kcal/mol more endothermic than $\mathbf{II_{MPC-E}}$.

In this mechanism, from $\mathbf{II_{MPC-I}}$, a water molecule ($H_2O^3$) bound to the Pd(II) ion is activated. Here, the $O^3$−$H^4$ bond of the water molecule is broken, and the proton is transferred to the $N^1$ atom of the Phe2 residue. This process occurs concomitantly with the transfer of the hydroxyl group (−$O^3$H) to the $C^2$ atom of the Phe1 residue and cleavage of the Phe1-Phe2 peptide bond. From $\mathbf{II_{MPC-I}}$, this process undergoes a barrier of 30.1 (30.6) kcal/mol; the optimized transition state ($\mathbf{TS(II-III)_{MPC}}$) is shown in Figure 9. The key bond distances (Pd−$O^3$ = 2.10, $O^3$−$H^4$ = 1.77, $N^1$−$H^4$ = 1.04, $O^3$−$C^2$ = 1.97, and $N^1$−$C^2$ = 1.58 Å) indicate that this process is concerted. Since this step is followed by a step ($\mathbf{II_{MPC-E}} \rightarrow \mathbf{II_{MPC-I}}$) that is endergonic by 5.3 (7.9) kcal/mol, the overall barrier from $\mathbf{II_{MPC-E}}$ becomes 35.4 (38.5) kcal/mol.

The computed barrier for the cleavage of the Phe1-Phe2 peptide bond by the artificial mononuclear Pd complex ($\mathbf{I_{MPC}}$) is found to be substantially higher than the natural enzymes; that is, 17.9 (24.1), 12.9 (16.6), and 11.0 (13.1) kcal/mol higher than MMP, BACE2, and IDE, respectively. Quite interestingly, this barrier is 2.9 (7.6), 3.8 (11.4), 4.4 (12.5), and 6.0 (10.5) kcal/mol lower than the ones previously calculated for the

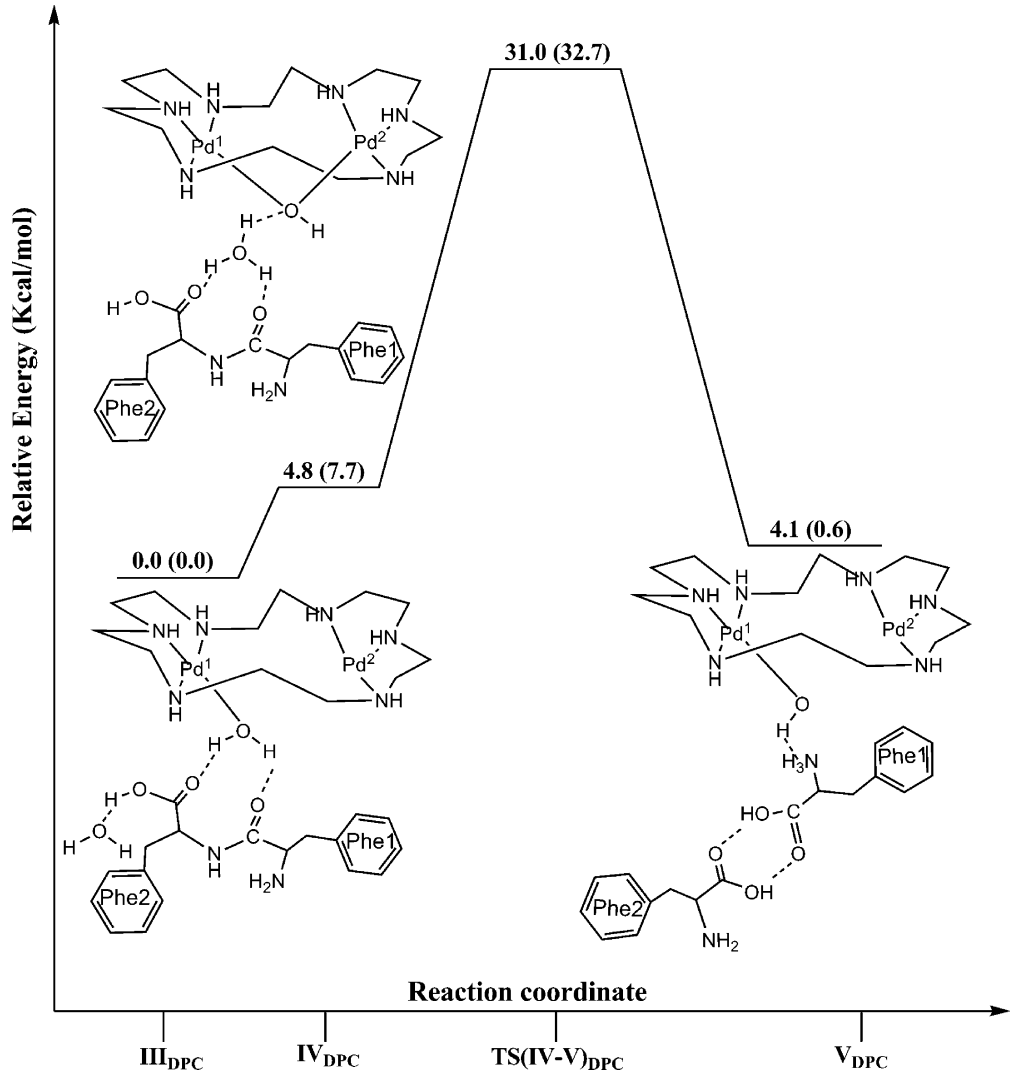


**Figure 14.** Potential energy diagram for peptide hydrolysis catalyzed by $[Pd_2(\mu\text{-OH})([18]aneN_6)]^{3+}$.

cleavages of the Gly-Pro-Met, Gly-Gly-Met, Gly-Sar-Met, and Gly-Pro-His bonds, respectively, by $\mathbf{I_{MPC}}$.[76] The cleavage of this bond leads to the carboxyl (−COOH) and amine ($-NH_2$) terminals of the Phe1-Phe2 peptide ($\mathbf{III_{MPC}}$) (Figure 9). In $\mathbf{III_{MPC}}$, the $N^1$ atom of the Phe2 side chain occupies the vacant location in the Pd(II) metal center. The generation of $\mathbf{III_{MPC}}$ is exothermic by 11.9 (2.2) kcal/mol from $\mathbf{II_{MPC\text{-}E}}$. However, the exothermicity of this reaction is 1.4 (0.10), 5.2 (1.0), and 16.6 (0.4) kcal/mol higher than MMP, BACE2, and IDE, respectively.

**IIId. Hydrolysis of Phe1-Phe2 Bond by $[Pd_2(\mu\text{-OH})([18]aneN_6)]^{3+}$ ($\mathbf{I_{DPC}}$) Complex.** The most energetically feasible mechanism for the cleavage of a peptide bond by $\mathbf{I_{DPC}}$ occurs through the activation of an external water molecule trapped between the substrate and the metal bound water molecule ($\mathbf{IId_{DPC}}$ in Figure 5). In the reactant of this mechanism ($\mathbf{III_{DPC}}$), the dipeptide (Phe1-Phe2) substrate coordinates through two strong hydrogen bonds with the water molecule ($H_2O^3$) bound only to one of the metal ($Pd^1$) ions ($O^3H^{12}-O^4 = 1.48$ and $O^3H-O^7 = 1.54$ Å) (Figure 10). In $\mathbf{III_{DPC}}$, the external water molecule ($H^{10}O^9H^{11}$), shown in the circle, that is utilized for the hydrolysis of the scissile peptide bond interacts with the carboxyl terminal group of the substrate via a hydrogen bond ($O^8H-O^9 = 1.44$ Å). In this structure, $Pd^1$ and $Pd^2$ contain 0.30 and 0.31*e* charges, respectively, and the metal−metal ($Pd^1-Pd^2$) bond distance is 2.76 Å.

In the next step, the water molecule moves adjacent to the cleavage site and abstracts a proton from the $Pd^1$ bound water molecule to generate a hydronium ion $(H_3O^9)^+$ that gets trapped between the hydroxyl ion ($-O^3H$) bridging between $Pd^1$ and $Pd^2$ and the substrate ($\mathbf{IV_{DPC}}$). The binding of the water molecule to the $Pd^1$ ion significantly reduces its $pK_a$ value and facilitates the formation of the hydronium ion. In $\mathbf{IV_{DPC}}$, the bridging hydroxyl group ($-O^3H$) is coordinated to both the Pd ions ($Pd^1-O^3 = 2.11$ and $Pd^2-O^3 = 2.20$ Å), and the $Pd^1-Pd^2$ distance is longer by 0.12 Å than $\mathbf{III_{DPC}}$. In comparison with $\mathbf{III_{DPC}}$, the charge on $Pd^2$ is also slightly increased by 0.02 e. In this structure, the hydronium ion is stabilized by three hydrogen bonds ($O^9H^{12}-O^3 = 1.61$, $O^9H^{10}-O^7 = 1.56$, and $O^9H^{11}-O^4 = 1.39$ Å), and the creation of this intermediate is endothermic by 4.8 (7.7) kcal/mol. In the final step, in a concerted manner, the $\mathbf{IV_{DPC}}$ intermediate collapses through the transfer of the $H^{10}$ proton to the $N^6$ nitrogen atom and the nucleophlic attack of the $-O^9H^{11}$ ion to the carbon ($C^5$) atom of the scissile peptide bond ($C^5-N^6$). The remaining $H^{12}$ proton subsequently moves back to the $Pd^1$ bound hydroxyl ion ($-O^3H$) to regenerate the metal−water ($Pd^1-H^{12}O^3H$) complex.

In the optimized transition state ($\mathbf{TS(IV-V)_{DPC}}$), the charge on the $Pd^1$ is increased by 0.05*e*, and all the key bond distances describe the concerted nature of this process ($O^3-H^{12} = 1.28$, $O^9-H^{12} = 1.16$, $O^9-C^5 = 1.70$, $N^6-H^{10} = 1.03$, and $O^5-N^6 = 1.66$ Å). This process takes place with the barrier of 31.0 (32.7) kcal/mol and leads to the cleavage of the $C^5-N^6$ peptide bond ($\mathbf{V_{DPC}}$). In $\mathbf{V_{DPC}}$, as a result of a proton transfer from the $Pd^1$ bound water molecule to the backbone amine ($-NH_2$) group of Phe1, only the hydroxyl group ($-O^3H$) is attached to this metal ion. The calculated barrier shows that the presence of the second metal ion ($Pd^2$) reduces the barrier for the hydrolysis of the peptide bond by 4.4 (5.8) kcal/mol than the mononuclear ($\mathbf{I_{MPC}}$) complex. This effect of the second metal center is similar to the one observed in the hydrolysis of phosphate esters, where dinuclear model complexes have been found to be more effective than the mononuclear ones.[106−108] However, the barrier for $\mathbf{I_{DPC}}$ is still higher by 13.5, 8.5, and 6.6 kcal/mol than the rate-determining steps in MMP, BACE2, and IDE enzymes. These results show that the rate of this reaction is still several orders of magnitudes slower than the one catalyzed by natural enzymes. The formation of the product is endothermic by 4.1 (0.6) kcal/mol, which is 16.0 kcal/mol less favorable than the $\mathbf{I_{MPC}}$ case.

## IV. Conclusions

In the present B3LYP study, mechanisms for the hydrolytic cleavage of the Phe1-Phe2 peptide bond have been investigated using the following three different types of catalysts: (1) aspartyl protease (($\beta$-secretase (BACE2)) (2) metallopeptidases (matrix metalloproteinase (MMP) and insulin degrading enzyme (IDE)) and (3) artificial peptidases ($[Pd(H_2O)_4]^{2+}$ ($\mathbf{I_{MPC}}$) and $[Pd_2(\mu\text{-}OH)([18]aneN_6)]^{3+}$, where $[18]aneN_6$ is 1,4,7,10,13,16-hexaazacyclooctadecane, ($\mathbf{I_{DPC}}$)). The potential energy surface (PES) diagrams for BACE2, MMP, $\mathbf{I_{MPC}}$, and $\mathbf{I_{DPC}}$ are shown in Figures 11−14, respectively, and for IDE, in Figure 5 of the Supporting Information.

The two active site aspartate residues (protonated Asp48 and unprotonated Asp241) containing BACE2 catalyze this reaction through the following two steps: (1) formation of the gem-diol intermediate and (2) cleavage of the Phe1-Phe2 peptide bond. The computed barriers, 20.1 (21.8) kcal/mol for step 1 and 22.5 (21.9) kcal/mol for step 2, are in good agreement with the measured barriers of ∼18 kcal/mol for both these steps for memapsin 2.[55] For BACE2, the collapse of the gem-diol intermediate ($\mathbf{II_{BACE2}}$) leading to the cleavage of the peptide bond was found to be the rate-limiting step.

On the other hand, a $Zn^{2+}$ metal center containing metallopeptidases (MMP and IDE) catalyzes this reaction through the following three steps: (1) activation of the metal bound water molecule, (2) formation of the gem-diol intermediate, and (3) cleavage of the peptide bond. In MMP, the generation of the gem-diol intermediate occurs with the barrier of 17.5 (14.4) kcal/mol and is calculated to be the rate-limiting step in the entire mechanism. The substitution of a His ligand with Glu in the $Zn^{2+}$ metal center of MMP generates the active site of IDE. In comparison with MMP, this substitution introduces significant structural and mechanistic changes in the catalytic cycle of IDE. For instance, in a marked difference from MMP, the activation of the water molecule in the first step becomes the rate-limiting process for IDE and occurs with a 6.9 (11.0) kcal/mol higher barrier than the rate-determining step of MMP.

The computed energetics for all the enzymes (BACE2. MMP, and IDE) are in good agreement with the measured and theoretical data.[55,67,69,71,64−104] Similar to MMP and IDE, both mono- and dinuclear-palladium-center-containing artificial peptidases $\mathbf{I_{MPC}}$ and $\mathbf{I_{DPC}}$, respectively, also utilize a metal-bound water molecule to hydrolyze the peptide bond. However, in the case of $\mathbf{I_{DPC}}$, an external water molecule trapped between the substrate and the $Pd^1$ metal-bound water molecule is more amenable to achieve this purpose. Although $\mathbf{I_{DPC}}$ catalyzes this reaction with a substantially high barrier (31.0 (32.7) kcal/mol), it was still found to be the better catalyst than $\mathbf{I_{MPC}}$ due to synergistic interactions between both metal ions ($Pd^1$ and $Pd^2$). $\mathbf{I_{MPC}}$ catalyzes it with an overall barrier of 35.4 (38.5) kcal/mol that is 4.4 (5.8) kcal/mol higher than $\mathbf{I_{DPC}}$.

The computed energetics predict that among all the catalysts used in this study, MMP is the fastest and $\mathbf{I_{MPC}}$ is the slowest catalyst in cleaving the Phe1-Phe2 peptide bond. However, on the basis of the computed energetics for this particular bond, it is not possible to accurately predict activities of the Pd-containing artificial peptidases ($\mathbf{I_{MPC}}$ and $\mathbf{I_{DPC}}$) in cleaving the other peptide bonds. For instance, IDE has previously been shown to hydrolyze the Lys-Gly, Phe-Phe and His-Gln peptide bonds with computed barriers of 14.3, 18.8, and 22.3 kcal/mol, respectively.[69]

These results have provided critical information concerning the exact roles of the microenvironments of active sites of the existing catalysts in the hydrolytic cleavage of a peptide bond. This information can be used to advance our efforts to design potent peptidases and catalytic drugs through modifications in the metal ion and ligand environment.

**Acknowledgment.** A funding grant (DOH Grant no. 08KN-11) to R.P. from the James and Esther King Biomedical Research Program of the Florida State Health Department is acknowledged.

**Supporting Information Available:** (a) Figures 1−5, (b) details of the MD simulations, and (c) Tables S1−S21: Cartesian coordinates (in Å) of all the optimized structures. This material is available free of charge via the Internet at http://pubs.acs.org.

## References and Notes

(1) Thomas, J. J.; Bakhtiar, R.; Siuzdak, G. *Acc. Chem. Res.* **2000**, *33*, 179.
(2) *Proteolytic Enzymes*; 2nd ed.; Beynon, R., Bond, J. S., Eds.; Oxford University Press: New York, 2001.
(3) Heyduk, T.; Baichoo, N.; Heyduk, E. *Met. Ions Biol. Syst.* **2001**, *38*, 255.
(4) Thorner, J.; Emr, S. D.; Abelson, J. N. *Methods Enzymol.* **2000**, *2000*, 326.
(5) Wallace, C. J. A. *Protein Engineering by Semisynthesis*; CRC Press: Boca Raton, FL, 2000.
(6) Suh, J. *Acc. Chem. Res.* **1992**, *25*, 273.
(7) Lee, T. Y.; Suh, J. *Chem. Soc. Rev.* **2009**, *38*, 1949.
(8) Suh, J.; Yoo, S. H.; Kim, M. G.; Jeong, K.; Ahn, J. Y.; Kim, M. S.; Chae, P.; Lee, T. Y.; Lee, J.; Lee, J.; Jang, Y. A.; Ko, E. H. *Angew. Chem., Int. Ed.* **2007**, *46*, 7064.
(9) Meggers, E. *Chem. Commun.* **2009**, 1001.
(10) Radzicka, A.; Wolfenden, R. *J. Am. Chem. Soc.* **1996**, *118*, 6105.
(11) Farzan, M.; Schnitzler, C. E.; Vasilieva, N.; Leung, D.; Choe, H. *Proc. Natl. Acad. Sci.* **2000**, *97*, 9712.
(12) Hussain, I.; Powell, D. J.; Howlett, D. R.; Chapman, G. A.; Golmour, L.; Murdock, P. R.; Tew, D. G.; Meek, T. D.; Chapman, C.; Schneider, K.; Ratcliffe, S. J.; Tettersall, D.; Testa, T. T.; Southan, C.; Ryan, D. M.; Simmons, D. L.; Walsh, F. S.; Dingwall, C.; Christie, G. *Mol. Cell. Neurosci.* **2000**, *16*, 609.
(13) Ostermann, N.; Eder, J.; Eidhoff, U.; Zink, F.; Hassiepen, U.; Worpenberg, S.; Maibaum, J.; Simic, O.; Hommel, U.; Gerhartz, B. *J. Mol. Biol.* **2006**, *355*, 249.
(14) Yan, R.; Bienkowski, M. E.; Shuck, M. E.; Miao, H.; Tory, M. C.; Pauley, A. M.; Brashler, J. R.; Stratman, N. C.; Mathews, W. R.; Buhl, A. E.; Carter, D. B.; Tomasselli, A. G.; Parodi, L. A.; Heinrikson, R. L.; Gurney, M. E. *Nature* **1999**, *402*, 533.

(15) Navia, M. A.; Fitzgerald, M. D. P.; Mckeever, B. M.; Leu, C.-T.; Heimbach, J. C.; Herber, W. K.; Sigal, I. S.; Darke, P. L.; Spronger, J. P. *Nature* **1989**, *337*, 615.
(16) Wlodawer, A.; Miller, M.; Jaskolski, M.; Sathyanarayana, B.; Baldwin, E.; Weber, I.; Selk, L.; Clawson, L.; Schneider, J.; Kent, S. *Science* **1989**, *245*, 616.
(17) Edbauer, D.; Winkler, E.; Regula, J. T.; Pesold, B.; Steiner, H.; Haass, C. *Nat. Cell Biol.* **2003**, *5*, 486.
(18) Kimberly, W. T.; LaVoie, M. J.; Ostaszewski, B. L.; Ye, W.; Wolfe, M. S.; Selkoe, D. J. *Proc. Natl. Acad. Sci. U.S.A.* **2003**, *100*, 6382.
(19) Takasugi, N.; Tomita, T.; Hayashi, I.; Tsuruoka, M.; Niimura, M.; Takahashi, Y.; Thinakaran, G.; Iwatsubo, T. *Nature* **2003**, *422*, 438.
(20) Kim, S. H.; Ikeuchi, T.; Yu, C.; Sisodia, S. S. *J. Biol. Chem.* **2003**, *278*, 33992.
(21) Bertini, I.; Calderone, V.; Fragai, M.; Luchinat, C.; Maletta, M.; Yeo, K. J. *Angew. Chem., Int. Ed.* **2006**, *45*, 7952.
(22) Browner, M. F.; Smith, W. W.; Castelhano, A. L. *Biochemistry* **1995**, *34*, 6602.
(23) Shen, Y.; Joachimiak, A.; Rosner, M. R.; Tang, W. J. *Nature* **2006**, *443*, 870.
(24) Im, H.; Manolopoulou, M.; Malito, E.; Shen, Y.; Zhao, J.; Neant-Fery, M.; Sun, C.-Y.; Meredith, S. C.; Sisodia, S. S.; Leissering, M. A.; Tang, W. J. *J. Biol. Chem.* **2007**, *282*, 25453.
(25) Milović, N. M.; Kostić, N. M. *J. Am. Chem. Soc.* **2003**, *125*, 781.
(26) Kumar, C. V.; Thota, J. *Inorg. Chem.* **2005**, *44*, 825.
(27) Rivas, J. C. M.; Salvagni, E.; Prabaharan, R.; Rosales, R. T. M.; Parsons, S. *Dalton Trans.* **2004**, 172.
(28) Rana, T. M.; Meares, C. F. *J. Am. Chem. Soc.* **1990**, *112*, 2457.
(29) Murthy, N. N.; Mahroof-Tahir, M.; Karlin, K. D. *J. Am. Chem. Soc.* **1993**, *115*, 10404.
(30) Suh, J. *Perspect. Bioinorg. Chem.* **1996**, *3*, 115.
(31) Milović, N. M.; Dutca, L.-M.; Kostić, N. M. *Chem.—Eur. J.* **2003**, *9*, 5097.
(32) Zhu, L.; Kostic, N. M. *J. Am. Chem. Soc.* **1993**, *115*, 4566.
(33) Yang, G.; Miao, R.; Li, Y.; Hong, J.; Zhao, C.; Guo, Z.; Zhu, L. *Dalton Trans.* **2005**, *9*, 1613.
(34) Sutton, P. A.; Buckingham, D. A. *Acc. Chem. Res.* **1987**, *20*, 357–364.
(35) Rana, T. M.; Meares, C. F. *Proc. Natl. Acad. Sci. U.S.A.* **1991**, *88*, 10578.
(36) Hohage, O.; Sheldrick, W. S. *J. Inorg. Biochem.* **2006**, *100*, 1506.
(37) Hohage, O.; Manka, S.; Sheldrick, W. S. *Inorg. Chim. Acta* **2009**, *362*, 953.
(38) Vicente, J.; Arcas, A. *Coord. Chem. Rev.* **2005**, *249*, 1135.
(39) Milović, N. M.; Kostić, N. M. *Met. Ions Biol. Syst.* **2001**, *38*, 145–186.
(40) Zhu, L.; Kostić, N. M. *Inorg. Chem.* **1992**, *31*, 3994.
(41) Kaminskaia, N. V.; Johnson, T. W.; Kostić, N. M. *J. Am. Chem. Soc.* **1999**, *121*, 8663–8664.
(42) Kaminskaia, N. V.; Kostić, N. M. *Inorg. Chem.* **2001**, *40*, 2368–2377.
(43) Parac, T. N.; Kostić, N. M. *J. Am. Chem. Soc.* **1996**, *118*, 5946–5951.
(44) Parac, T. N.; Kostić, N. M. *J. Am. Chem. Soc.* **1996**, *118*, 51–58.
(45) Lipscomb, W. N.; Strater, N. *Chem. Rev.* **1996**, *96*, 2375.
(46) Christianson, D. W.; Lipscomb, W. N. *Acc. Chem. Res.* **1989**, *22*, 62.
(47) Duckworth, W. C.; Bennett, R. G.; Hamel, F. G. *Endocr. Rev.* **1998**, *19*, 608.
(48) Leissring, M. A.; Lu, A.; Condron, M. A.; Teplow, D. B.; Stein, R. L.; Farris, W.; Selkoe, D. J. *J. Biol. Chem.* **2003**, *278*, 37314.
(49) Bora, R. P.; Prabhakar, R. *Biochemistry* **2010**, *49*, 3947.
(50) Pearl, L.; Blundell, T. *FEBS Lett.* **1984**, *174*, 96.
(51) Suguna, K.; Padlan, E. A.; Smith, C. W.; Carlson, W. D.; Davies, D. R. *Proc. Natl. Acad. Sci. U.S.A.* **1987**, *84*, 7009.
(52) Rodriguez, E. J.; Angeles, T. S.; Meek, T. D. *Biochemistry* **1993**, 12380.
(53) Meek, T. D.; Rodriguez, E. J.; Angeles, T. S. *Methods Enzymol.* **1994**, *241*, 127.
(54) Brown, R. S.; Bennet, A. J.; Slebocka-Tilk, H. *Acc. Chem. Res.* **1992**, *25*, 481.
(55) Lin, X.; Koelsch, G.; Wu, S.; Downs, D.; Dashti, A.; Tang, J. *Proc. Natl. Acad. Sci. U.S.A.* **2000**, *97*, 1456.
(56) Cascella, M.; Micheletti, C.; Rothlisberger, U.; Carloni, P. *J. Am. Chem. Soc.* **2005**, *127*, 3734.
(57) Chatfield, D.; Eurenius, C. P.; Brooks, K.; Bernard, R. *J. Mol. Struct.: THEOCHEM* **1998**, *423*, 79.
(58) Piana, S.; Bucher, D.; Carloni, P.; Rothlisberger, U. *J. Phys. Chem. B* **2004**, *108*, 11139.
(59) Trylska, J.; Grochowski, P.; McCammon, J. A. *Protein Sci.* **2004**, *13*, 513.
(60) Bjelic, S.; Åqvist, J. *Biochemistry* **2006**, *45*, 7709.
(61) Bjelic, S.; Åqvist, J. *Biochemistry* **2004**, *43*, 14521.
(62) Singh, R.; Barman, A.; Prabhakar, R. *J. Phys. Chem. B* **2009**, *113*, 2990.
(63) Lowther, W. T.; Matthews, B. W. *Chem. Rev.* **2002**, *102*, 4581.
(64) Apiyo, D.; Zhao, Li.; Tsai, M.-D.; Selby, T. L. *Biochemistry* **2005**, *44*, 9980.
(65) Tseng, B. P.; Esler, W. P.; Clish, C. B.; Stimson, E. R.; Ghilardi, J. R.; Vinters, H. V.; Mantyh, P. W.; Lee, J. P.; Maggio, J. E. *Biochemistry* **1999**, *38*, 10424.
(66) Neant-Fery, M.; Ordoñez, Logan, T. P.; Selkoe, D. J.; Li, L.; Reinstatler, L.; Leissring, M. A. *Proc. Natl. Acad. Sci. U.S.A.* **2008**, *105*, 9582.
(67) Pelmenschikov, V.; Siegbahn, P. E. M. *Inorg. Chem.* **2002**, *41*, 5659.
(68) Díaz, N.; Suárez, D. *J. Phys. Chem. B* **2008**, *112*, 8412.
(69) Bora, R. P.; Ozbil, M.; Prabhakar, R. *J. Biol. Inorg. Chem.* **2010**, *15*, 485.
(70) Amata, O.; Marino, T.; Russo, N.; Toscano, M. *J. Am. Chem. Soc.* **2009**, *131*, 14804.
(71) Pelmenschikov, V.; Blomberg, M. R. A.; Siegbahn, P. E. M. *J. Biol. Inorg. Chem.* **2002**, *7*, 284.
(72) Antonczak, S.; Monard, G.; Ruiz-Lopez, M. F.; Rivail, J. L. *J. Am. Chem. Soc.* **1998**, *120*, 8825.
(73) Antonczak, S.; Monard, G.; Ruiz-Lopez, M. F.; Rivail, J. L. *J. Mol. Model.* **2000**, *6*, 527.
(74) Glades, A., Vallee, B. L. *Metal Ions in Biological Systems*; Dekker: New York, 1983; Vol. 15.
(75) Milović, N. M.; Kostić, N. M. *J. Am. Chem. Soc.* **2002**, *124*, 4759–4769.
(76) Kumar, A.; Zhu, X.; Walsh, K.; Prabhakar, R. *Inorg. Chem.* **2010**, *49*, 38.
(77) Milović, N. M.; Kostić, N. M. *J. Am. Chem. Soc.* **2003**, *125*, 781.
(78) Hong, L.; Koelsch, G.; Lin, X.; Wu, S.; Terzyan, S.; Ghosh, A. K.; Zhang, X. C.; Tang, J. *Science* **2000**, *290*, 150.
(79) Guex, N.; Peitsch, M. C. *Electrophoresis* **1997**, *18*, 2714.
(80) Coates, L.; Erskine, P. T.; Mall, S.; Gill, R.; Wood, S. P.; Myles, D. A.; Cooper, J. B. *Eur. Biophys. J.* **2006**, *35*, 559.
(81) Coates, L.; Tuan, H.-F.; Tomanicek, S.; Kovalevsky, A.; Mustyakimov, M.; Erskine, P. T.; Cooper, J. B. *J. Am. Chem. Soc.* **2008**, *130*, 7235.
(82) Yu, N.; Hayik, S. A.; Wang, B.; Liao, N.; Reynolds, C. H.; Merz, K. M. *J. Chem. Theory Comput.* **2006**, *2*, 1057.
(83) Krieger, E.; Vriend, G. *Bioinformatics* **2002**, *18*, 315.
(84) Berendsen, H. J. C.; van der Spoel, D.; van Drunen, D. *Comput. Phys. Commun.* **1995**, *91*, 43.
(85) Lindahl, E.; Hess, B.; van der Spoel, D. *J. Mol. Model.* **2001**, *7*, 306.
(86) Oostenbrink, C.; Villa, A.; Mark, A. E.; Van Gunsteren, W. F. *J. Comput. Chem.* **2004**, *25*, 1656.
(87) Berendsen, H. J. C.; Postma, J. P. M.; van Gunsteren, W. F.; Hermans, J. *Interation Models for Water in Relation to Protein Hydration*; D. Reider Publishing Company, Dordrecht, 1981.
(88) Miyamoto, S.; Kollman, P. A. *J. Comput. Chem.* **1992**, *13*, 952.
(89) Hess, B.; Bekker, H.; Berendsen, H. J. C.; Fraaije, J. G. E. M. *J. Comput. Chem.* **1997**, *18*, 1463.
(90) Darden, T. A.; York, D.; Pedersen, L. *J. Chem. Phys.* **1993**, *98*, 10089.
(91) York, D. M.; Wlodawer, A.; Pedersen, L. G.; Darden, T. A. *Proc. Natl. Acad. Sci. U.S.A.* **1994**, *91*, 8715.
(92) Humphrey, W.; Dalke, A.; Schulten, K. *J. Mol. Graphics* **1996**, *14*, 33.
(93) Prabhakar, R.; Morokuma, K.; Musaev, D. G. *Biochemistry* **2006**, *45*, 6967.
(94) Siegbahn, P. E. M.; Blomberg, M. R. A. *Chem. Rev.* **2000**, *100*, 421.
(95) Prabhakar, R.; Vreven, T.; Morokuma, K.; Musaev, D. G. *Biochemistry* **2005**, *44*, 11864.
(96) Himo, F.; Siegbahn, P. E. M. *Chem. Rev.* **2003**, *103*, 2421.
(97) Frisch, M. J.; Trucks, G. W.; Schlegel, H. B.; Scuseria, G. E.; Robb, M. A.; Cheeseman, J. R.; Montgomery, J. A., Jr.; Vreven, T.; Kudin, K. N.; Burant, J. C.; Millam, J. M.; Iyengar, S. S.; Tomasi, J.; Barone, V.; Mennucci, B.; Cossi, M.; Scalmani, G.; Rega, N.; Petersson, G. A.; Nakatsuji, H.; Hada, M.; Ehara, M.; Toyota, K.; Fukuda, R.; Hasegawa, J.; Ishida, M.; Nakajima, T.; Honda, Y.; Kitao, O.; Nakai, H.; Klene, M.; Li, X.; Knox, J. E.; Hratchian, H. P.; Cross, J. B.; Bakken, V.; Adamo, C.; Jaramillo, J.; Gomperts, R.; Stratmann, R. E.; Yazyev, O.; Austin, A. J.; Cammi, R.; Pomelli, C.; Ochterski, J. W.; Ayala, P. Y.; Morokuma, K.; Voth, G. A.; Salvador, P.; Dannenberg, J. J.; Zakrzewski, V. G.; Dapprich, S.; Daniels, A. D.; Strain, M. C.; Farkas, O.; Malick, D. K.; Rabuck, A. D.; Raghavachari, K.; Foresman, J. B.; Ortiz, J. V.; Cui, Q.; Baboul, A. G.; Clifford, S.; Cioslowski, J.; Stefanov, B. B.; Liu, G.; Liashenko, A.; Piskorz, P.; Komaromi, I.; Martin, R. L.; Fox, D. J.; Keith, T.; Al-Laham, M. A.; Peng, C. Y.; Nanayakkara, A.; Challacombe, M.; Gill, P. M. W.; Johnson,

B.; Chen, W.; Wong, M. W.; Gonzalez, C. Pople, J. A. *Gaussian 03 C.02 ed.*; Gaussian, Inc.: Wallingford, CT, 2004.
(98) Becke, A. D. *Phys. Rev. A* **1988**, *38*, 3098.
(99) Becke, A. D. *J. Chem. Phys.* **1993**, *98*, 5648.
(100) Lee, C.; Yang, W.; Parr, R. G. *Phys. Rev. B* **1988**, *37*, 785.
(101) Hay, P. J.; Wadt, W. R. *J. Chem. Phys.* **1985**, *82*, 270.
(102) Cances, E.; Mennucci, B.; Tomasi, J. *J. Chem. Phys.* **1997**, *107*, 3032.
(103) Polgar, L.; Szeltner, Z.; Boros, I. *Biochemistry* **1994**, *33*, 9351.
(104) Morihara, K.; Hiroshige, T. *Eur. J. Biochem.* **1970**, *15*, 374.
(105) Pelmenschikov, V.; Siegbahn, P. E. M. *Inorg. Chem.* **2002**, *41*, 5659.
(106) Bruice, T. C.; Tsubouchi, A.; Dempcy, R. O.; Olson, L. P. *J. Am. Chem. Soc.* **1996**, *118*, 9867.
(107) Hegg, E. L.; Burstyn, J. N. *Coord. Chem. Rev.* **1998**, *173*, 133.
(108) Liu, C.; Wang, M.; Zhang, T.; Sun, H. *Coord. Chem. Rev.* **2004**, *248*, 147.

JP104294X